MOBO-OSD: Batch Multi-Objective Bayesian Optimization via Orthogonal Search Directions

Lam Ngo

School of Computing Technologies RMIT University, Australia tung.lam.ngo@rmit.edu.au

Jeffrey Chan

School of Computing Technologies RMIT University, Australia jeffrey.chan@rmit.edu.au

Huong Ha

School of Computing Technologies RMIT University, Australia huong.ha@rmit.edu.au

Hongyu Zhang

School of Big Data and Software Engineering Chongqing University, China hyzhang@cqu.edu.cn

Abstract

Bayesian Optimization (BO) is a powerful tool for optimizing expensive blackbox objective functions. While extensive research has been conducted on the single-objective optimization problem, the multi-objective optimization problem remains challenging. In this paper, we propose MOBO-OSD, a multi-objective Bayesian Optimization algorithm designed to generate a diverse set of Pareto optimal solutions by solving multiple constrained optimization problems, referred to as MOBO-OSD subproblems, along orthogonal search directions (OSDs) defined with respect to an approximated convex hull of individual objective minima. By employing a well-distributed set of OSDs, MOBO-OSD ensures broad coverage of the objective space, enhancing both solution diversity and hypervolume performance. To further improve the density of the set of Pareto optimal candidate solutions without requiring an excessive number of subproblems, we leverage a Pareto Front Estimation technique to generate additional solutions in the neighborhood of existing solutions. Additionally, MOBO-OSD supports batch optimization, enabling parallel function evaluations to accelerate the optimization process when resources are available. Through extensive experiments and analysis on a variety of synthetic and real-world benchmark functions with two to six objectives, we demonstrate that MOBO-OSD consistently outperforms the state-of-the-art algorithms. Our code implementation can be found at https://github.com/LamNgo1/mobo-osd.

1 Introduction

Multi-objective Bayesian Optimization (MOBO) has recently attracted much attention [5, 13, 52, 44, 1]. MOBO extends Bayesian Optimization (BO) — a powerful framework for optimizing expensive black-box functions — to settings where multiple, often conflicting, objectives must be optimized simultaneously. Applications of MOBO include but are not limited to machine learning [47, 29], material design [18, 56], agriculture [27, 28], robotics [54, 34] and vehicle design [32, 2].

There are several challenges when working with MOBO problems. First, the objective functions are often conflicting, meaning that improving one objective may deteriorate another. Hence the goal is not to identify a single optimal solution, but rather a set of *Pareto optimal solutions*. Second, maintaining the diversity among these Pareto optimal solutions is crucial to capture the wide range of trade-off across all objectives. This becomes more challenging under the limited evaluation budget in MOBO settings, where there is less budget to balance between exploration and exploitation while

covering the Pareto front. Third, batch optimization plays an important role in reducing the time and cost through parallel evaluations of objective functions. However, in MOBO, it introduces additional complexity, as it requires modeling the interactions among unobserved points across multiple objective functions. Fourth, the computational cost remains a significant drawback, as the cost for training surrogate models and computing multi-objective acquisition functions, e.g., EHVI [13], become increasingly expensive with the number of objectives. Despite the growing body of MOBO research, there exists substantial room for improvement. Many existing approaches rely on scalarization techniques [5, 9, 41], which often fail to capture a diverse Pareto front, leading to suboptimal performance in terms of the hypervolume indicator. Moreover, several studies are unable to scale to a large number of objectives (M > 3) [33] or suffer from high computational cost in batch optimization settings [13, 52].

In this paper, our goal is to develop a novel MOBO algorithm that prioritizes Pareto front diversity, resulting in an improvement in hypervolume performance and scalability to an arbitrary number of objectives in both sequential and batch optimization settings. To achieve this, we build upon the key insight of the Normal Boundary Intersection (NBI) method [11]: the intersection points between the boundary of the objective space and the vectors orthogonal to the convex hull of individual minima (CHIM) of the objectives could be Pareto optimal solutions. This geometric approach has been shown to generate a well-distributed (diverse) set of Pareto optimal solutions and scale well to a large number of objectives in multi-objective optimization problems with a large evaluation budget. To incorporate this idea under the limited evaluation budget in MOBO problems, we first introduce a technique to effectively approximate the CHIM. We then generate a well-distributed set of orthogonal search directions (OSDs) with respect to the approximated CHIM and define a tailored search procedure that solves a constrained single-objective optimization problem along each OSD (MOBO-OSD subproblem) to identify intersection points with the boundary that are likely to be Pareto optimal. By constructing a well-distributed set of OSDs, MOBO-OSD achieves broad coverage of the objective space, enhancing both solution diversity and hypervolume performance. To further enrich the set of Pareto optimal candidate solutions without the need to solve a large number of MOBO-OSD subproblems, we incorporate a Pareto Front Estimation (PFE) technique [46] that locally explores the neighborhood of existing Pareto optimal candidates. All candidates are aggregated and evaluated using the hypervolume improvement acquisition function [19], and those with the highest scores are selected as the next batch of data points for evaluation. Finally, to support batch optimization, we incorporate the Kriging Believer technique [22] while considering the diversity of exploration regions, i.e., ensuring that selected points for observation originate from different exploration spaces. We name our method Batch Multi-Objective Bayesian Optimization via Orthogonal Search Directions (MOBO-OSD). Our thorough analysis and extensive experiments on various synthetic and real-world benchmark problems, in both sequential and batch optimization settings, show that MOBO-OSD outperforms the state-of-the-art MOBO methods. We summarize our contributions as follows.

- We propose MOBO-OSD, a novel MOBO algorithm that generates a diverse set of Pareto optimal candidate solutions by solving multiple optimization subproblems defined along search directions orthogonal to the approximated CHIM of the objective space. To further enhance the diversity, we propose to locally explore the Pareto set for additional Pareto solutions via a PFE technique.
- We develop MOBO-OSD in such a way that it can perform effectively in the batch optimization setting by leveraging the Kriging Believer technique and exploration space information.
- We demonstrate that MOBO-OSD can outperform the state-of-the-art MOBO baselines on a comprehensive set of synthetic and real-world multi-objective benchmark problems with a wide range of numbers of objectives, in both sequential and batch settings.

2 Background

2.1 Multi-Objective Optimization

We consider a multi-objective optimization (MOO) problem involving a *vector-valued* objective function $\mathbf{f}: \mathcal{X} \to \mathcal{Y}$ with $\mathbf{f} = (f_1, \dots, f_M)$, where $\mathcal{X} \subset \mathbb{R}^D$ is a D-dimensional input space, and $\mathcal{Y} \subset \mathbb{R}^M$ is an M-dimensional output space (M > 1). Without loss of generality, we assume the goal is to minimize all objectives of \mathbf{f} . In MOO, it is generally not possible to find a single solution that optimizes all objectives simultaneously. Instead, the aim is to identify the set of *Pareto optimal solutions*, where no objective can be improved without deteriorating at least one of the others.

A solution $\mathbf{f}(\mathbf{x}^{(i)})$ is said to *Pareto dominate* another solution $\mathbf{f}(\mathbf{x}^{(j)})$, i.e., $\mathbf{f}(\mathbf{x}^{(i)}) \succ \mathbf{f}(\mathbf{x}^{(j)})$, if $f_m(\mathbf{x}^{(i)}) \geq f_m(\mathbf{x}^{(j)}) \ \forall m=1,\ldots,M$ and there exists $m' \in \{1,\ldots,M\}$ such that $f_m(\mathbf{x}^{(i)}) > f_m(\mathbf{x}^{(j)})$. The set of Pareto optimal solutions is called the *Pareto front* $\mathcal{P}_f = \{\mathbf{f}(\mathbf{x}) \mid \nexists \mathbf{x}' \in \mathcal{X} : \mathbf{f}(\mathbf{x}') \succ \mathbf{f}(\mathbf{x})\}$, and the corresponding set of Pareto optimal inputs is called the *Pareto set* $\mathcal{P}_s = \{\mathbf{x} \in \mathcal{X} \mid \mathbf{f}(\mathbf{x}) \in \mathcal{P}_f\}$. Formally, the MOO problem is expressed as finding the Pareto front \mathcal{P}_f and Pareto set \mathcal{P}_s such that,

$$\mathcal{P}_f \in \min_{\mathbf{x} \in \mathcal{X}} (f_1(\mathbf{x}), f_2(\mathbf{x}), \dots, f_M(\mathbf{x})). \tag{1}$$

To measure the quality of a Pareto front \mathcal{P}_f , the *Hypervolume* (HV) indicator [59] is one of the most widely used metrics [45, 5, 9, 13, 4, 1]. Given a reference point $\mathbf{r} \in \mathbb{R}^M$, the HV indicator of a finite approximated Pareto front \mathcal{P}_f is defined as the M-dimensional Lebesgue measure λ_M of the space dominated by solutions \mathbf{p} in \mathcal{P}_f and upper bounded by the reference point \mathbf{r} . Formally, $\mathrm{HV}(\mathcal{P}_f,\mathbf{r}) = \lambda_M(\bigcup_{\mathbf{p}\in\mathcal{P}_f}[\mathbf{r},\mathbf{p}])$, where $[\mathbf{r},\mathbf{p}]$ denotes the hyperrectangle bounded by the reference point \mathbf{r} and $\mathbf{p} \in \mathcal{P}_f$ [9, 13, 14]. The higher the HV, the better \mathcal{P}_f approximates the true Pareto front.

2.2 Multi-Objective Bayesian Optimization

Bayesian Optimization [21] is a common tool for optimizing *expensive black-box* objective functions f. Given a minimization problem, the goal is to find the global optimum of the function f using the least function evaluations. BO sequentially selects observation data via an iterative process. Each BO iteration trains a probabilistic *surrogate model*, builds an *acquisition function*, then selects the acquisition function's maximizer as the next observation. The most common type of surrogate model for BO is a Gaussian Process (GP) [55], which provides a posterior distribution over the objective function given the observed dataset \mathcal{D} . The acquisition function $\alpha: \mathcal{X} \to \mathbb{R}$ is constructed from the surrogate model and an optimization policy to quantify the utility of each unobserved data point. Single-objective BO has many common acquisition functions such as EI [37], UCB [48] and TS [51].

Multi-objective Bayesian Optimization (MOBO) extends the capabilities of BO to optimize *expensive* black-box vector-valued objective functions $\mathbf{f}:\mathcal{X}\to\mathcal{Y}$ with $\mathbf{f}=(f_1,\ldots,f_M)$. Given a minimization problem, the goal is to find the Pareto set \mathcal{P}_s and the corresponding Pareto front \mathcal{P}_f , using the least function evaluations. In MOBO, the most common surrogate model is a set of GPs, where each GP independently represents an objective function f_m [31, 9, 41, 5, 13]. For acquisition functions, while several works leverage existing single-objective acquisition functions [31, 41, 5], others propose new acquisition functions tailored for the MOO setting [23, 4, 52, 13, 14, 12].

3 Related Work

There have been various works aiming to develop MOBO algorithms. Many works have attempted to adapt single-objective (SO) acquisition functions to the multi-objective optimization (MOO) framework. One of the earliest methods is ParEGO [31], which randomly scalarizes the objectives and applies the EI acquisition function [37] to determine the next data points for observation. Paria et al. [41] systematically generalize the random scalarization technique, allowing different scalarization techniques, e.g., weighted sum and Tchebyshev [39], as well as different SO acquisition functions, e.g., TS [51], UCB [48], to be integrated into the MOBO framework. TSEMO [9] formulates a multiobjective TS acquisition function [51] by sampling all objectives, employs NSGA-II [16] to solve the resulting optimization problem, and selects the next evaluations by maximizing hypervolume improvement. USeMO [5] aims to maximize the uncertainty reduction of the candidate points generated by a MO acquisition function, which is defined by applying SO acquisition functions to each objective GP. Recently, PDBO [1] uses a multi-armed bandit technique to select an SO acquisition function and generate a candidate pool, followed by a Determinantal Point Process to select a diverse set of solutions. Our proposed method operates directly on a multi-objective (MO) acquisition function, the Hypervolume Improvement, which is more suitable for the MOBO setting. In the experimental section, we compare against ParEGO, USeMO and PDBO - one of the latest state-of-the-art methods.

There are also many works that have focused on developing new acquisition functions tailored for the MOO setting. Information-theoretic (IT) MO acquisition functions aim to maximize the information gain of the next observation about the objective functions. Examples include PESMO [23],

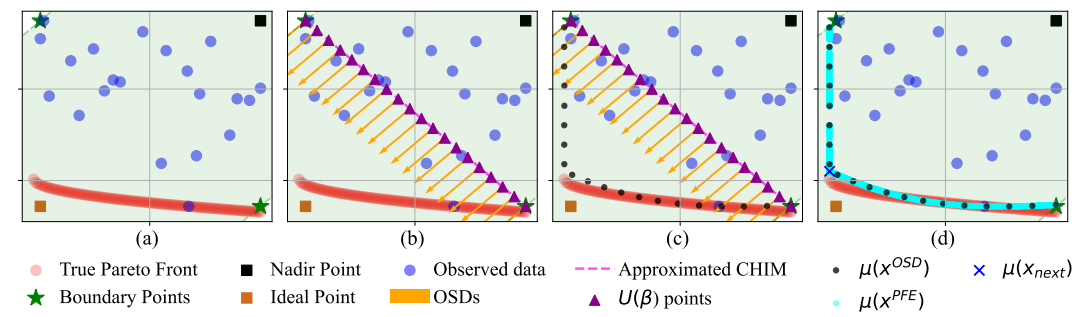


Figure 1: **Summary of the MOBO-OSD algorithm:** (a) The boundary points are defined via the nadir and ideal points; (b) The approximated CHIM is defined from the boundary points and the OSDs are defined on each $\mathcal{U}(\beta)$ point and orthogonal to the approximated CHIM; (c) The MOBO-OSD subproblem (Eq. (2)) is optimized for \mathbf{x}^{OSD} candidates; (d) Additional candidates \mathbf{x}^{PFE} are generated by locally exploring around \mathbf{x}^{OSD} . Finally, \mathbf{x}_{next} is chosen based on Eq. (4).

MESMO [4], PFES [49], and JES [52]. PAL [61] is another algorithm based on information theory, but it is only applicable to input spaces with finite set of discrete points. Another widely used approach to define MO acquisition functions is through the HV indicator. The EHVI acquisition function [19] extends the EI concept from SOO to compute the expected improvement in the hypervolume of the Pareto front. Daulton et al. [13] propose a novel formulation of EHVI in a parallel setting, namely qEHVI, based on Monte-Carlo sampling. Despite being differentiable, even for M>2objectives, qEHVI can suffer from high computational cost. Unlike qEHVI, which computes the expected hypervolume improvement under the posterior distribution, DGEMO [33] relies solely on the hypervolume improvement of the posterior mean, yet its integration with the Pareto Front Estimation technique [46] renders the method competitive. Nonetheless, unlike our proposed method, its search strategy for Pareto optimal solutions is entirely random and does not ensure adequate coverage of the Pareto front. Moreover, DGEMO requires a specialized data structure that must be designed separately for each specific number of objectives, thereby limiting its scalability beyond problems with three objectives. Recently, the HVKG [12] acquisition function, which extends the SO Knowledge Gradient acquisition function, has been proposed to tackle multi-fidelity and decoupled MOO problems. Although our proposed method uses the Hypervolume Improvement acquisition function, it is compatible with alternative MO acquisition functions, rendering it applicable to new developments. In the experiment section, we compare against JES - a state-of-the-art IT-based method, as well as qEHVI and DGEMO, as they also leverage the HV-based acquisition functions.

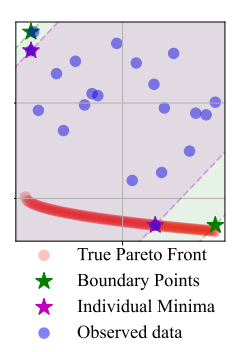
Evolutionary Algorithms (EA) are also capable of tackling MOO problems. Examples of multiobjective Evolutionary Algorithms include MOEA/D [57], SMS-EMOA [6], and NSGA-II [16, 26]. Generally, EA-based algorithms are less sample-efficient than BO-based methods, making them unsuitable for settings with a limited evaluation budget. We compare against NSGA-II, the most widely used EA baseline in MOBO works.

4 Proposed Method

In this section, we present our proposed algorithm MOBO-OSD. See Fig. 1 for a summary of the proposed MOBO-OSD method. The core idea of MOBO-OSD is to find the Pareto optimal solutions by estimating the intersection points between the boundary of the objective space and the vectors orthogonal to the convex hull of individual objective minima (CHIM) [11]. To achieve this in the MOBO setting with limited evaluation budget, we first approximate the CHIM using a bounded hyperplane (the *approximated CHIM*), and then construct a set of well-distributed orthogonal search directions (OSDs) w.r.t. this approximated CHIM (Sec. 4.1). Then we propose the *MOBO-OSD subproblem* for each OSD (Sec. 4.2), followed by the incorporation of the Pareto Front Estimation technique (Sec. 4.3). Finally, we propose the batch selection process (Sec. 4.4). For simplicity, we assume that all the objective values are non-negative, which can be achieved by offsetting the current worst value found so far in each objective.

4.1 The MOBO-OSD Components

Approximated CHIM. As it is not possible to obtain the individual minima of the objectives in MOBO settings with a limited evaluation budget, we propose to approximate the CHIM as a convex hull of M boundary points, which are the extreme points computed from the observed dataset. Denote the ideal point $\mathbf{y}^{\text{ideal}} = (\min_{\mathbf{x} \in \mathcal{D}} f_1(\mathbf{x}), \dots, \min_{\mathbf{x} \in \mathcal{D}} f_M(\mathbf{x}))$ and the nadir point $\mathbf{y}^{\text{nadir}} = (\max_{\mathbf{x} \in \mathcal{D}} f_1(\mathbf{x}), \dots, \max_{\mathbf{x} \in \mathcal{D}} f_M(\mathbf{x}))$ as M-dimensional points whose components are the best and the worst values observed so far for each objective, respectively. Then, the m-th boundary point \mathbf{p}_m is computed by replacing the m-th component of the ideal point with its corresponding nadir value, leaving the rest unchanged, i.e., \mathbf{p}_m satisfies $[\mathbf{p}_m]_j = [\mathbf{y}^{\text{nadir}}]_j$ if j = m and $[\mathbf{y}^{\text{ideal}}]_j$ otherwise, for $j = 1, \dots, M$. This approximated CHIM serves as a replacement for the true CHIM, which is not available as individual

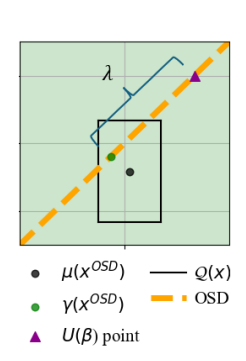


minima cannot be found efficiently in MOBO settings. Compared to a simpler alternative, which approximates the CHIM via individual minima found so far in the observed dataset, our approach avoids prematurely shrinking the search region for the Pareto optimal solutions. In the alternative method, if a good Pareto optimal solution is found early, the individual minima found so far in the observed dataset immediately shrink the search region, overlooking other potential unexplored regions of the objective space to find more Pareto optimal solutions. In contrast, the proposed approximated CHIM maintains a broader search region, allowing our proposed method MOBO-OSD to explore more promising regions. See the inset for an example where our proposed approximated CHIM provides a larger search region (green area) than that of the alternative method (purple area).

Orthogonal Search Directions. Having obtained the approximated CHIM, the Orthogonal Search Direction (OSD) is defined as a one-dimensional line in the objective space that follows the unit normal vector n of the approximated CHIM and passes through a point on the approximated CHIM. Denote β as an M-dimensional convex combination vector $\beta \in \mathbb{R}^M$, $\sum_{m=1}^M \beta_m = 1$ and $\beta_m > 0$, which defines a point on the approximated CHIM $\mathcal{U}(\beta)$. Formally, $\mathcal{U}(\beta) = \{\mathbf{P}\beta = \sum_{m=1}^M \beta_m \mathbf{p}_m \mid \beta \in \mathcal{U}\}$ $\mathbb{R}^M, \sum_{m=1}^M \beta_m = 1, \beta_m > 0$ such that $\mathbf{P} = [\mathbf{p}_1, \dots, \mathbf{p}_M]$ is the matrix whose columns are the M boundary points p_m . We then denote the OSD as a line $\mathcal{L}(\mathcal{U}(\beta), \mathbf{n})$ that goes through the point $\mathcal{U}(\beta)$ in the direction of the normal vector **n**. In order to generate a well-distributed set of OSDs, it is essential to construct a well-distributed set of $\mathcal{U}(\beta)$ points. This is equivalent to generating a well-distributed set of $\{\beta\}$ over an M-dimensional unit simplex, as $\mathcal{U}(\beta)$ is, by definition, the linear transformation of β from a unit simplex to the approximated CHIM. To achieve this, we propose to employ the Riesz s-Energy method [8] to arrange the set of β in a well-distributed fashion. Following the physics principle that the minimum potential energy state of a set of points corresponds to a diverse distribution of those points, the Riesz s-Energy aims to minimize the sum of a potential energy function defined over $\{\beta\}$, which effectively generates a well-distributed set of β . To sum up, in practice, we generate n_{β} well-distributed OSDs by first producing n_{β} well-distributed convex combination weight vectors $\{\beta_i\}$, then linearly mapping them to the corresponding points $\mathcal{U}(\beta_i)$ on the approximated CHIM, and finally defining the set of OSDs $\{\mathcal{L}(\mathcal{U}(\beta_i), \mathbf{n})\}\$, where $i = 1, \dots, n_{\beta}$. See Fig. 1b for an illustration of the OSDs. More details on the OSDs are in Appendix A.3.

4.2 The MOBO-OSD Subproblem

We now present the MOBO-OSD subproblem, which is a constrained optimization problem designed to obtain the Pareto optimal solutions by finding the intersection between an OSD and the boundary of the objective space. Given a convex combination weight vector $\boldsymbol{\beta}$, a point on the approximated CHIM $\mathcal{U}(\boldsymbol{\beta})$, and an OSD $\mathcal{L} = \mathcal{L}(\mathcal{U}(\boldsymbol{\beta}), \mathbf{n})$, the intersection point \mathbf{L}^* between the line \mathcal{L} and the boundary of the objective space can be parameterized as $\mathbf{L}^* = \mathcal{U}(\boldsymbol{\beta}) + \lambda^* \mathbf{n}$, where the scalar parameter λ^* satisfies $(\mathbf{x}^*, \lambda^*) \in \max_{\lambda \in \mathbb{R}, \mathbf{x} \in \mathcal{X}} \lambda$ subject to $\mathcal{U}(\boldsymbol{\beta}) + \lambda \mathbf{n} = \mathbf{f}(\mathbf{x})$. This is the ideal optimization subproblem used in the NBI method. More details on the NBI technique and its subproblem can be found in Appendix A.1. In MOBO settings, however, it is not feasible to solve this ideal constrained problem due to the high evaluation cost of the constraints. Therefore, we propose the MOBO-OSD subproblem, which aims to approximate λ^*



and \mathbf{x}^* . We modify the ideal problem as follows. First, we replace the objective function values $\mathbf{f}(\mathbf{x})$ with the estimated function values, the posterior mean vector $\boldsymbol{\mu}(\mathbf{x})$. Second, we relax the equality constraint that forces $\boldsymbol{\mu}(\mathbf{x})$ to be exactly on the OSD, $\mathcal{U}(\boldsymbol{\beta}) + \lambda \mathbf{n} = \boldsymbol{\mu}(\mathbf{x})$, and only require $\boldsymbol{\mu}(\mathbf{x})$ to be within a certain distance from the OSD. This can be achieved by constraining the projection of $\boldsymbol{\mu}(\mathbf{x})$ within its confidence bounds, i.e., $\gamma(\mathbf{x}; \boldsymbol{\beta}, \mathbf{n}) \in \mathcal{Q}(\mathbf{x})$ where $\gamma(\mathbf{x}; \boldsymbol{\beta}, \mathbf{n})$ is the projection function of $\boldsymbol{\mu}(\mathbf{x})$ onto the OSD \mathcal{L} , and $\mathcal{Q}(\mathbf{x}) = \{\mathbf{y} \mid \boldsymbol{\mu}(\mathbf{x}) - \delta \boldsymbol{\sigma}(\mathbf{x}) \leq \mathbf{y} \leq \boldsymbol{\mu}(\mathbf{x}) + \delta \boldsymbol{\sigma}(\mathbf{x})\}$ represents a hyper-rectangular confidence region defined by the posterior standard deviation vector $\boldsymbol{\sigma}$ and a scaling factor δ [61]. Finally, we maximize the scalar λ , which represents the scalar parameter corresponding to the projection point on the OSD \mathcal{L} , i.e., $\gamma(\mathbf{x}; \boldsymbol{\beta}, \mathbf{n}) = \mathcal{U}(\boldsymbol{\beta}) + \lambda \mathbf{n}$. See the inset for an illustration of the MOBO-OSD subproblem. Note that λ is not necessarily the distance $\|\gamma(\mathbf{x}) - \mathcal{U}(\boldsymbol{\beta})\|_2$, as λ can be negative in the case of a concave Pareto front, e.g., the DTLZ2 benchmark function [17]. Ultimately, the MOBO-OSD subproblem is defined as the following constrained optimization problem,

$$(\mathbf{x}^{\text{OSD}}, \lambda^{\text{OSD}}) \in \max_{\mathbf{x} \in \mathcal{X}} \lambda \quad \text{subject to} \quad \begin{cases} \mathbf{g}_1(\mathbf{x}) = \gamma(\mathbf{x}; \boldsymbol{\beta}, \mathbf{n}) - \boldsymbol{\mu}(\mathbf{x}) + \delta \boldsymbol{\sigma}(\mathbf{x}) \ge \mathbf{0} \\ \mathbf{g}_2(\mathbf{x}) = \boldsymbol{\mu}(\mathbf{x}) + \delta \boldsymbol{\sigma}(\mathbf{x}) - \gamma(\mathbf{x}; \boldsymbol{\beta}, \mathbf{n}) \ge \mathbf{0} \end{cases} . \tag{2}$$

A detailed formula for λ can be derived from the definition of the projection operator, i.e., $\gamma(\mathbf{x}; \boldsymbol{\beta}, \mathbf{n}) = \operatorname{Proj}_{\mathcal{L}}(\boldsymbol{\mu}(\mathbf{x})) = \operatorname{Proj}_{\mathbf{n}}(\boldsymbol{\mu}(\mathbf{x}) - \mathcal{U}(\boldsymbol{\beta})) = \mathcal{U}(\boldsymbol{\beta}) + \frac{(\boldsymbol{\mu}(\mathbf{x}) - \mathcal{U}(\boldsymbol{\beta})) \cdot \mathbf{n}}{\mathbf{n} \cdot \mathbf{n}} \mathbf{n}$. Therefore, λ can be expressed as $\lambda(\mathbf{x}; \boldsymbol{\beta}, \mathbf{n}) = (\boldsymbol{\mu}(\mathbf{x}) - \mathcal{U}(\boldsymbol{\beta})) \cdot \mathbf{n}$, as $\|\mathbf{n}\| = 1$. Solving Eq. (2) results in $(\mathbf{x}^{\text{OSD}}, \lambda^{\text{OSD}})$, which approximates the ideal $(\mathbf{x}^*, \lambda^*)$ as Eq. (2) ensures that the obtained solution has competitive estimated function values while remaining close to the current OSD \mathcal{L} . The point $\boldsymbol{\mu}(\mathbf{x}^{\text{OSD}})$ serves as an approximation of the intersection point \mathbf{L}^* . Given a set of $n_{\boldsymbol{\beta}}$ well-distributed OSDs as defined in Sec. 4.1, solving a MOBO-OSD subproblem for each OSD \mathcal{L} generates a well-distributed set of solutions $\{\mathbf{x}^{\text{OSD}}\}$. See Fig. 1c for an illustration.

The detailed optimization routine for the proposed MOBO-OSD subproblem in Eq. (2) proceeds as follows. We solve Eq. (2) using a gradient-based off-the-shelf optimizer, e.g., SLSQP [35]. To compute the gradient vector $\mathcal{J}_{\lambda}(\mathbf{x})$ and Jacobian matrix $\mathcal{J}_{[\mathbf{g}_1,\mathbf{g}_2]}(\mathbf{x})$, we require the Jacobian matrix of the posterior mean and standard deviation vectors of the GPs, which can be computed either in analytic form under common kernels [33, 38] or by automatic differentiation via computational graphs [42]. Moreover, since the problem is highly non-convex, we solve Eq. (2) via multiple starting points $\{\mathbf{x}_i^{(0)}\}_{i=0}^{n_s}$ and select the most promising solution among the resulting solutions. Specifically, for each starting point $\mathbf{x}_i^{(0)}$, we obtain a solution $\mathbf{x}_i^{\mathrm{OSD}}(\boldsymbol{\beta}) = \mathbf{x}_i^{\mathrm{OSD}}$ that exhibits a different trade-off between maximizing $\lambda(\mathbf{x})$ and minimizing the distance from $\mu(\mathbf{x})$ to \mathcal{L} , i.e., $l(\mathbf{x}) = \|\mu(\mathbf{x}) - \gamma(\mathbf{x})\|_2$. Since it is not feasible to find the promising solution $\mathbf{x}_i^{\mathrm{OSD}}$ that maximizes $\lambda(\mathbf{x}_i^{\mathrm{OSD}})$ while enforcing $l(\mathbf{x}_i^{\mathrm{OSD}}) = 0$, we opt to select the most potential solution by formulating a bi-objective selection step to identify the best trade-off among the n_s candidates $\{\mathbf{x}_i^{\mathrm{OSD}}\}_{i=1}^{n_s}$, characterized by $\lambda_i = \lambda(\mathbf{x}_i^{\mathrm{OSD}})$ and $l_i = l(\mathbf{x}_i^{\mathrm{OSD}})$. We use the hypervolume indicator for this selection, computing the hypervolume contribution for each pair $[\lambda_i, l_i]$ is the reduction in hypervolume when that pair is removed from the solution set $\mathbf{S} = \{[\lambda_i, l_i]_{i=1}^{n_s}$. Formally, HVC $([\lambda_i, l_i]) = \mathrm{HV}(\mathbf{S}, \mathbf{r}_s) - \mathrm{HV}(\mathbf{S} \setminus [\lambda_i, l_i], \mathbf{r}_s)$, where $\mathbf{r}_s = \mathbf{s}^{\mathrm{nadir}} + 0.1 \cdot (\mathbf{s}^{\mathrm{nadir}} - \mathbf{s}^{\mathrm{ideal}})$ is the reference point computed from the nadir point $\mathbf{s}^{\mathrm{nadir}}$ and the ideal point $\mathbf{s}^{\mathrm{ideal}}$ of the set \mathbf{S} . The final solution for Eq. (2) is chosen as $\mathbf{x}_{i}^{\mathrm{OSD}}(\boldsymbol{\beta}) = \mathbf{x}_{i}^{\mathrm{OSD}}$, where $i^* = \arg\max_{i=1,\dots,n_s}$

4.3 Pareto Front Estimation

For each MOBO-OSD subproblem (corresponding to a point on the approximated CHIM $\mathcal{U}(\beta)$), we obtain a solution $\mathbf{x}^{\text{OSD}}(\beta)$ (in Eq. (2)). Instead of discretizing the approximated CHIM into a large number of points $\mathcal{U}(\beta)$, we propose to leverage a Pareto Front Estimation (PFE) technique to explore the local region around the current solution $\mathbf{x}^{\text{OSD}}(\beta)$ and generate additional data points that are expected to be Pareto optimal. One successful approach is the First Order Approximation technique [46, 33], which computes a local exploration space $\mathcal T$ around a current Pareto optimal solution. Specifically, we consider the First Order Approximation problem, in which the surrogate model is used to estimate the exploration space $\mathcal T$ around the solution $\mathbf{x}^{\text{OSD}}(\beta)$. See Appendix A.2 for an overview of the First Order Approximation method. In particular, solving the First Order Approximation problem results in a set of directions \mathbf{v} , which define the space $\mathcal T$. Then we estimate

Algorithm 1 The MOBO-OSD Algorithm

```
1: Input: Objective function f(.), evaluation budget T, batch size b, number of weight vectors n_{\beta}
 2: Output: The Pareto set \mathcal{P}_s
 3: Initialize data points and append to the observed dataset \mathcal D
 4: while t \leq T do
 5:
            Compute approximated CHIM and define n_{\beta} OSDs
                                                                                                                                                    ⊳ Sec. 4.1
            Train GPs for each objective function f_m
 6:
            for each point \mathcal{U}(\boldsymbol{\beta}) on the approximated CHIM \mathbf{do}
 7:
                  Optimize the MOBO-OSD subproblem to generate a candidate \mathbf{x}^{\text{OSD}}(\boldsymbol{\beta}) \triangleright \text{Eq. (2)}
Estimate the Pareto front around \mathbf{x}^{\text{OSD}}(\boldsymbol{\beta}) to explore more candidates \mathbf{x}^{\text{PFE}}(\boldsymbol{\beta}) \triangleright \text{Eq. (3)}
Append \mathbf{X}_c \leftarrow \mathbf{X}_c \cup \mathbf{x}^{\text{PFE}}(\boldsymbol{\beta})
 8:
 9:
10:
11:
            Select a batch of b solutions from \mathbf{X}_c and evaluate them; Increase t \leftarrow t + b
12:
                                                                                                                                                       ⊳ Eq. (4)
13: end while
14: Return \mathcal{P}_s from dataset \mathcal{D}
```

the Pareto Front by randomly sampling n_e data points in \mathcal{T} such that,

$$\mathbf{X}^{\text{PFE}}(\boldsymbol{\beta}) = \{\mathbf{x}_i^{\text{PFE}}(\boldsymbol{\beta})\} = \{\mathbf{x}^{\text{OSD}}(\boldsymbol{\beta}) + \mathbf{u}_i \mathbf{v}\} \text{ for } i = 1, \dots, n_e,$$
(3)

where \mathbf{u}_i is the *i*-th random perturbation term to shift the solution \mathbf{x}^{OSD} along the directions \mathbf{v} . This PFE step generates additional candidate points around the current expected Pareto optimal candidates \mathbf{x}^{OSD} from the previous step. This also helps to avoid solving an excessive number of MOBO-OSD subproblems that are close to one another. See the ablation study in Sec. 5.2 for details.

This step is repeated for all MOBO-OSD subproblems, i.e., for each point on the approximated CHIM $\mathcal{U}(\boldsymbol{\beta})$, resulting in a set of candidates $\mathbf{X}_c = \bigcup_{i=1}^{n_{\boldsymbol{\beta}}} \mathbf{X}^{\text{PFE}}(\boldsymbol{\beta}_i)$, where $n_{\boldsymbol{\beta}}$ denotes the number of weight vectors $\boldsymbol{\beta}$ on the approximated CHIM. In general, $|\mathbf{X}_c| = n_{\boldsymbol{\beta}} \times n_e$.

4.4 Batch Selection Strategy

Having generated $n_{\beta} \times n_e$ candidate solutions \mathbf{X}_c , we use the Hypervolume Improvement (HVI) of the posterior mean as the acquisition function to determine the most promising solutions to be evaluated - solutions that are expected to maximize the hypervolume contribution [9, 33]. Given the current approximate Pareto front \mathcal{P}_f computed from the observed dataset \mathcal{D} and a reference point \mathbf{r} , the HVI acquisition function is defined as $\alpha_{\mathrm{HVI}}(\mathbf{x};\mathcal{P}_f,\mathbf{r}) = \mathrm{HV}(\boldsymbol{\mu}(\mathbf{x}) \cup \mathcal{P}_f,\mathbf{r}) - \mathrm{HV}(\mathcal{P}_f,\mathbf{r})$, where $\boldsymbol{\mu}(.)$ is the posterior mean function. For batch selection, the goal is to pick a batch of b data points \mathbf{X}_b that achieve high HVI values while maintaining diversity among the chosen solutions. To address the problem, first, we apply the Kriging Believer (KB) method [22] to improve the posterior mean estimation given unobserved data points during batch selection. In particular, after selecting a data point \mathbf{x}_i for $i \in [1, \dots, b]$, we re-train the GP models on the aggregated dataset $\mathcal{D} \cup \{\mathbf{x}_i, \boldsymbol{\mu}(\mathbf{x}_i)\}$. Secondly, we boost the diversity by choosing candidate points coming from different exploration spaces \mathcal{T} . This is because the approximated candidate points from a single exploration space \mathcal{T} tend to be close to one another [46], therefore exhibiting similar contributions to the hypervolume. Denote $\psi(\beta_i, \mathbf{X})$ as a function that counts the number of candidates $\mathbf{x} \in \mathbf{X}$ originating from the exploration space \mathcal{T} around $\mathbf{x}^{\mathrm{OSD}}(\beta_i)$. Hence, the batch selection mechanism is formulated as follows,

$$\mathbf{X}_b = \underset{\mathbf{X}_b \in \mathbf{X}_c}{\operatorname{argmax}} \ \alpha_{\text{HVI}}(\mathbf{x}; \mathcal{P}_f, \mathbf{r}) \quad \text{such that } \max_{i=1,\dots,n_\beta} \psi(\boldsymbol{\beta}_i, \mathbf{X}_b) - \min_{i=1,\dots,n_\beta} \psi(\boldsymbol{\beta}_i, \mathbf{X}_b) \leq 1. \tag{4}$$

The constraints in Eq. (4) are designed to ensure that the number of data points selected from different exploration spaces differs by at most one. In practice, we solve Eq. (4) sequentially to select b data points \mathbf{X}_b from the candidate set \mathbf{X}_c . In each iteration, after re-training the GP models (as required by KB) and selecting the best candidate point based on α_{HVI} , we remove from \mathbf{X}_c all other candidates originating from the same exploration space, then repeat the process to select the next point in the batch. If the candidate set \mathbf{X}_c becomes empty, all previously removed but unselected candidate points are reintroduced, and the process is repeated.

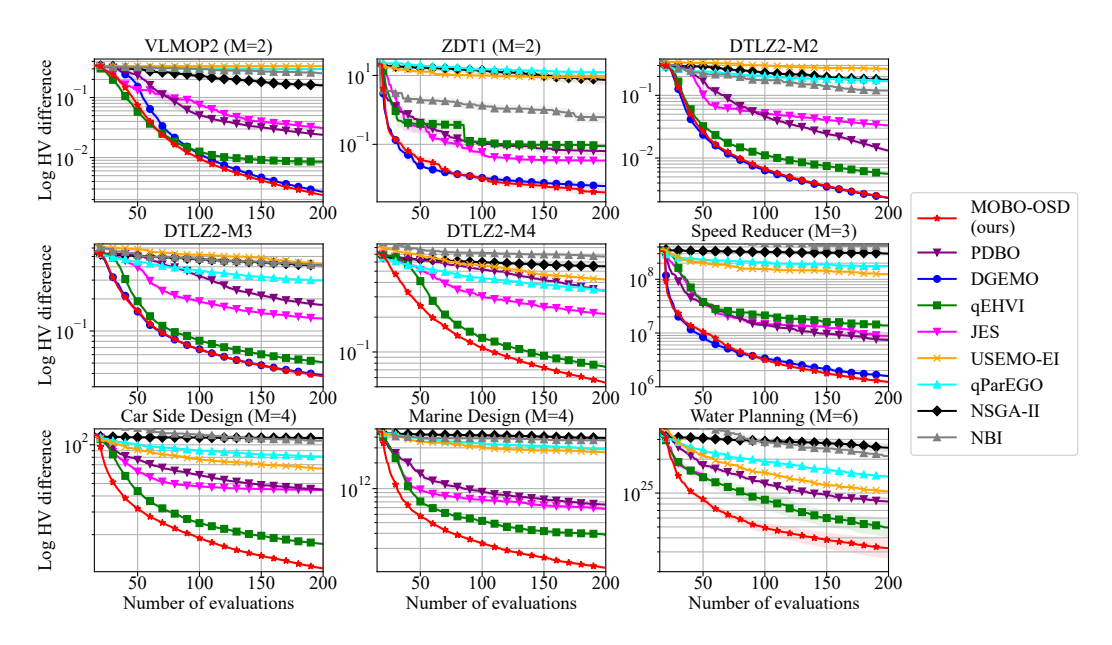


Figure 2: Comparison of MOBO-OSD against the SOTA baselines on 5 synthetic and 4 real-world benchmark problems in sequential setting (batch size 1). Note that DGEMO does support problems with M>3 objectives. Overall, MOBO-OSD outperforms the baselines.

4.5 Overall Algorithm

The overall MOBO-OSD algorithm is described in Alg. 1. MOBO-OSD operates in an iterative fashion. In each iteration, based on the observed dataset \mathcal{D} , we compute M boundary points \mathbf{P} , the approximated CHIM \mathcal{U} , and the n_{β} OSDs (line 5). Subsequently, for each point $\mathcal{U}(\beta)$ on the approximated CHIM, we optimize the MOBO-OSD subproblem to generate a Pareto optimal candidate \mathbf{x}^{OSD} , and then locally explore the space around \mathbf{x}^{OSD} to generate additional Pareto optimal candidates \mathbf{x}^{PFE} (lines 8 - 9). We then use the aggregated set of candidates \mathbf{X}_c from all n_{β} OSDs to select a batch of b solutions using the α_{HVI} acquisition function and the exploration space constraint (line 12). The process is repeated until the evaluation budget is exhausted, and the final Pareto front \mathcal{P}_f and Pareto set \mathcal{P}_s are computed from the observed dataset \mathcal{D} .

5 Experiments

Now we empirically evaluate our proposed method, MOBO-OSD, against the state-of-the-art methods on an extensive set of synthetic and real-world benchmark problems.

Experimental Settings and Baselines. We evaluate the proposed algorithm **MOBO-OSD** against a comprehensive set of baselines: **qParEGO** [31], **USeMO** [5], **DGEMO** [33], **PDBO** [1], **JES** [52], **qEHVI** [13], **NSGA-II** [16] and **NBI** [11]. For USeMO, we select the EI acquisition function as it has good performance and is commonly used in other works. For qParEGO, we use the batch implementation developed by Daulton et al. [13]. For DGEMO, we note that the authors' implementation only supports problems with M=2 and M=3 objectives. For JES, due to its prohibitive computational cost (Appendix A.11), we only compare under the sequential optimization setting (batch size 1). For NBI, to the best of our knowledge, no open-source implementation of the method currently exists; therefore, we re-implemented it following the procedure described in [11]. Detailed implementations of MOBO-OSD and the baselines can be found in Appendix A.7.

For the comparison metrics, we compute the logarithmic hypervolume difference between the hypervolume of the best accumulated observed Pareto front and the maximum hypervolume. The hypervolume is calculated using the reference points **r** specified in Appendix A.6. We report the mean and the standard error across 10 independent runs.

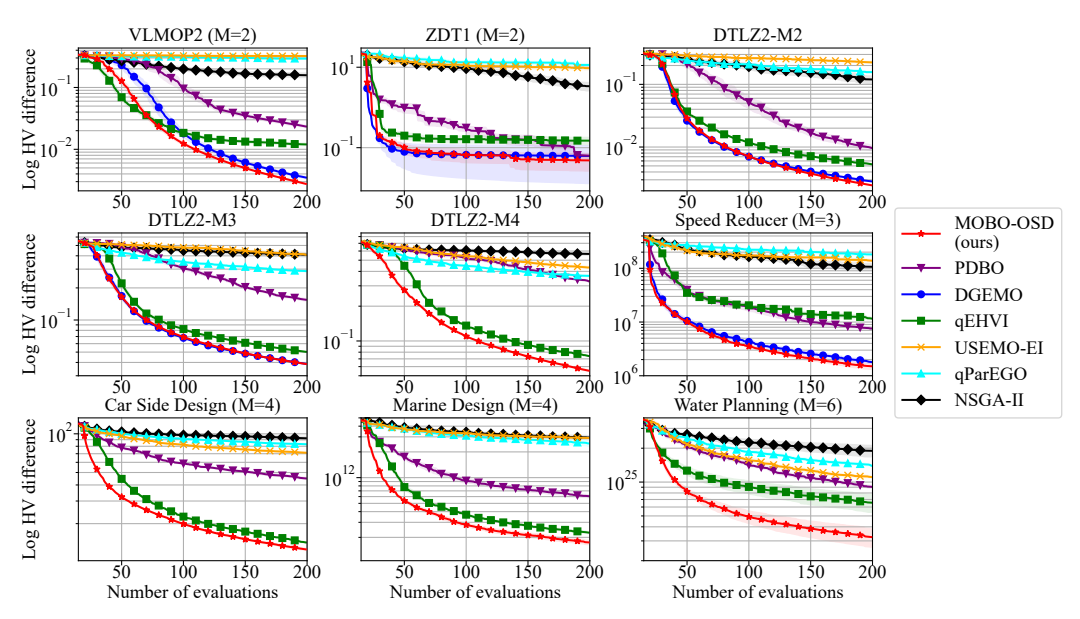


Figure 3: Comparison of MOBO-OSD against the SOTA baselines on 5 synthetic and 4 real-world benchmark problems in batch setting (batch size 4). Overall, MOBO-OSD outperform the baselines.

Benchmark Problems. We conduct experiments on five synthetic and four real-world multiobjective benchmark problems. The number of objectives ranges from two to six, which is common in the MOBO literature. For synthetic benchmark problems, we use DTLZ2 with different objective settings $M \in \{2,3,4\}$ [17], ZDTI [15], and VLMOP2 [53]. For real-world benchmark problems, we use various problems from the RE problem suite [50] including Speed Reducer, Car Side Design, Marine Design, and Water Planning. The dimensionality and number of objective settings for each function are given in Table 2. These problems are widely used in the MOBO literature [5, 9, 13, 12, 1, 33]. Details of the benchmark problems can be found in Appendix A.6.

5.1 Comparison with Baselines

Sequential Optimization. Fig. 2 shows the performance of all baselines on all nine benchmark problems in the sequential setting (batch size 1). Across all benchmark problems, both synthetic and real-world, MOBO-OSD consistently outperforms other state-of-the-art methods. qEHVI shows competitive performance in most cases, yet eventually finds suboptimal solutions. DGEMO also shows strong performance, but is outperformed by MOBO-OSD on VLMOP2 and Speed Reducer. Moreover, it is limited to problems with at most three objectives $M \leq 3$. NSGA-II often cannot compete with the MOBO algorithms in the case of limited evaluation budget. These results indicate the efficiency of MOBO-OSD in achieving fast convergence towards the Pareto front.

Batch Optimization. We conduct experiments in batch settings, with batch size $b = \{4, 8, 10\}$. Fig. 3 shows the performance of all baselines across all nine benchmark problems with batch size 4, whereas additional batch results can be found in Appendix A.8. Similar to the batch size 1 setting, MOBO-OSD consistently outperforms other state-of-the-art methods. qEHVI and DGEMO remain the two strongest baselines after MOBO-OSD, achieving hypervolume results close to those of MOBO-OSD. This result further emphasizes the efficiency of MOBO-OSD, even in the batch setting. Furthermore, we provide a theoretical time complexity analysis for MOBO-OSD, along with a runtime comparison between MOBO-OSD and the baselines in Appendix A.11, demonstrating the scalability of MOBO-OSD to an arbitrary number of objectives in both sequential and batch settings.

5.2 Ablation Study

In this section, we conduct a study on the effect of the n_{β} parameter - the number of points on the approximate CHIM $\mathcal{U}(\beta)$ - on the performance of MOBO-OSD. A larger n_{β} corresponds to a denser set of points on the approximated CHIM. We evaluate MOBO-OSD using varying

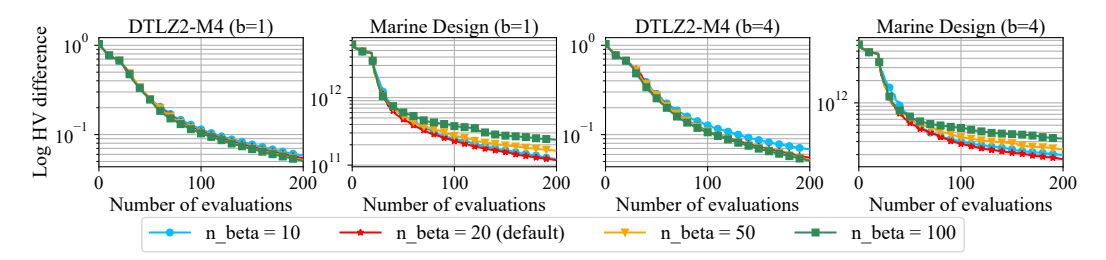


Figure 4: Ablation study on the effect of parameter n_{β} . Full results can be found in the Appendix A.9. Overall, MOBO-OSD is robust against n_{β} .

values of $n_{\beta} \in \{10, 50, 100\}$ on all nine benchmark problems and compare to the default setting $(n_{\beta} = 20)$. Four representative results are shown in Fig. 4, while the remaining results can be found in Appendix A.9. Fig. 4 shows that MOBO-OSD's overall performance remains stable across different values of n_{β} , indicating the robustness of the proposed algorithm with respect to this parameter.

We hypothesize that this robustness can be attributed to the Pareto Front Estimation (PFE) component (Sec. 4.3), which facilitates the generation of additional Pareto optimal candidates. Without the component, MOBO-OSD would require more $\mathcal{U}(\beta)$ points, thus solving a larger number of MOBO-OSD subproblems to achieve a comparable set of Pareto optimal candidates. To validate this hypothesis, we conduct a study by removing the PFE component and run the resulting MOBO-OSD variant with varying values of $n_{\beta} \in \{20, 100, 200, 500\}$. As shown in Table 1, increasing n_{β} leads to performance improvements. This finding suggests that although PFE enhances the efficiency of MOBO-OSD, it is not an essential component, as similar performance can be attained by increasing the density of the $\mathcal{U}(\beta)$ set.

Table 1: Ablation results (in HV) on the effect of n_{β} on MOBO-OSD without the PFE component.

MOBO-OSD method	DTLZ2-M2	VLMOP2	Car Side Design
W/o PFE $(n_{\beta}=20)$	0.4041 ± 0.0004	0.2713 ± 0.0020	145.1195 ± 0.3340
W/o PFE ($n_{\beta} = 100$)	0.4118 ± 0.0001	0.2978 ± 0.0011	154.3249 ± 0.2662
W/o PFE ($n_{\beta} = 200$)	0.4142 ± 0.0001	0.3076 ± 0.0006	157.2311 ± 0.2095
W/o PFE ($n_{\beta} = 500$)	0.4164 ± 0.0001	0.3159 ± 0.0004	160.2797 ± 0.2118
Default (with PFE)	0.4217 ± 0.0000	0.3383 ± 0.0000	177.4782 ± 0.2310

6 Conclusions

In this paper, we address the multi-objective Bayesian optimization problem for expensive black-box, vector-valued objective functions. We propose MOBO-OSD, a novel algorithm that aims to generate a well-distributed set of solutions via multiple subproblems defined along orthogonal search directions. To further enrich the diversity of the solutions, we perform local exploration around current Pareto optimal candidates, generating additional Pareto optimal candidate solutions. These candidates are scored using the Hypervolume Improvement acquisition function, while batch selection is guided by the Kriging Believer strategy and the exploration space information. Our experimental results show that MOBO-OSD outperforms state-of-the-art methods across various synthetic and real-world benchmark problems with varying number of objectives, in both sequential and batch settings.

Limitations. One limitation of our approach is that it focuses on noiseless observations, a common assumption in various existing works. Future work could address this limitation by employing acquisition functions that can handle noise and by improving the MOBO-OSD subproblem - for example, by integrating the uncertainty of previous observations when defining the projection.

Acknowledgments

The first author (L.N.) would like to thank the School of Computing Technologies, RMIT University, Australia and the Google Cloud Research Credits Program for providing computing resources for this project. Additionally, this project was undertaken with the assistance of computing resources from RMIT Advanced Cloud Ecosystem (RACE).

References

- [1] Alaleh Ahmadianshalchi, Syrine Belakaria, and Janardhan Rao Doppa. Pareto front-diverse batch multi-objective bayesian optimization. In *Proceedings of the AAAI Conference on Artificial Intelligence*, volume 38, pages 10784–10794, 2024.
- [2] Siwakorn Anosri, Natee Panagant, Pakin Champasak, Sujin Bureerat, Chinnapat Thipyopas, Sumit Kumar, Nantiwat Pholdee, Betül Sultan Yıldız, and Ali Riza Yildiz. A comparative study of state-of-the-art metaheuristics for solving many-objective optimization problems of fixed wing unmanned aerial vehicle conceptual design. *Archives of Computational Methods in Engineering*, 30(6):3657–3671, 2023.
- [3] Maximilian Balandat, Brian Karrer, Daniel R. Jiang, Samuel Daulton, Benjamin Letham, Andrew Gordon Wilson, and Eytan Bakshy. BoTorch: A Framework for Efficient Monte-Carlo Bayesian Optimization. In *Advances in Neural Information Processing Systems* 33, 2020.
- [4] Syrine Belakaria, Aryan Deshwal, and Janardhan Rao Doppa. Max-value entropy search for multi-objective bayesian optimization. *Advances in neural information processing systems*, 32, 2019.
- [5] Syrine Belakaria, Aryan Deshwal, Nitthilan Kannappan Jayakodi, and Janardhan Rao Doppa. Uncertainty-aware search framework for multi-objective bayesian optimization. In *Proceedings of the AAAI Conference on Artificial Intelligence*, volume 34, pages 10044–10052, 2020.
- [6] Nicola Beume, Boris Naujoks, and Michael Emmerich. Sms-emoa: Multiobjective selection based on dominated hypervolume. *European journal of operational research*, 181(3):1653–1669, 2007.
- [7] J. Blank and K. Deb. pymoo: Multi-objective optimization in python. *IEEE Access*, 8:89497–89509, 2020.
- [8] Julian Blank, Kalyanmoy Deb, Yashesh Dhebar, Sunith Bandaru, and Haitham Seada. Generating well-spaced points on a unit simplex for evolutionary many-objective optimization. *IEEE Transactions on Evolutionary Computation*, 25(1):48–60, 2020.
- [9] Eric Bradford, Artur M Schweidtmann, and Alexei Lapkin. Efficient multiobjective optimization employing gaussian processes, spectral sampling and a genetic algorithm. *Journal of global optimization*, 71(2):407–438, 2018.
- [10] Carlos A Coello Coello and Gary B Lamont. *Applications of multi-objective evolutionary algorithms*, volume 1. World Scientific, 2004.
- [11] Indraneel Das and John E Dennis. Normal-boundary intersection: A new method for generating the pareto surface in nonlinear multicriteria optimization problems. *SIAM journal on optimization*, 8(3):631–657, 1998.
- [12] Sam Daulton, Maximilian Balandat, and Eytan Bakshy. Hypervolume knowledge gradient: a lookahead approach for multi-objective bayesian optimization with partial information. In *International Conference on Machine Learning*, pages 7167–7204. PMLR, 2023.
- [13] Samuel Daulton, Maximilian Balandat, and Eytan Bakshy. Differentiable expected hypervolume improvement for parallel multi-objective bayesian optimization. *Advances in Neural Information Processing Systems*, 33:9851–9864, 2020.
- [14] Samuel Daulton, Maximilian Balandat, and Eytan Bakshy. Parallel bayesian optimization of multiple noisy objectives with expected hypervolume improvement. *Advances in Neural Information Processing Systems*, 34:2187–2200, 2021.
- [15] Kalyanmoy Deb. Multi-objective genetic algorithms: Problem difficulties and construction of test problems. *Evolutionary computation*, 7(3):205–230, 1999.
- [16] Kalyanmoy Deb and Himanshu Jain. An evolutionary many-objective optimization algorithm using reference-point-based nondominated sorting approach, part i: solving problems with box constraints. *IEEE transactions on evolutionary computation*, 18(4):577–601, 2013.

- [17] Kalyanmoy Deb, Lothar Thiele, Marco Laumanns, and Eckart Zitzler. Scalable test problems for evolutionary multiobjective optimization. In *Evolutionary multiobjective optimization:* theoretical advances and applications, pages 105–145. Springer, 2005.
- [18] Aryan Deshwal, Cory M Simon, and Janardhan Rao Doppa. Bayesian optimization of nanoporous materials. *Molecular Systems Design & Engineering*, 6(12):1066–1086, 2021.
- [19] Michael Emmerich and Jan-willem Klinkenberg. The computation of the expected improvement in dominated hypervolume of pareto front approximations. *Rapport technique, Leiden University*, 34:7–3, 2008.
- [20] Jacob Gardner, Geoff Pleiss, Kilian Q Weinberger, David Bindel, and Andrew G Wilson. Gpytorch: Blackbox matrix-matrix gaussian process inference with gpu acceleration. *Advances in neural information processing systems*, 31, 2018.
- [21] Roman Garnett. Bayesian optimization. Cambridge University Press, 2023.
- [22] David Ginsbourger, Rodolphe Le Riche, and Laurent Carraro. Kriging is well-suited to parallelize optimization. In *Computational intelligence in expensive optimization problems*, pages 131–162. Springer, 2010.
- [23] Daniel Hernández-Lobato, Jose Hernandez-Lobato, Amar Shah, and Ryan Adams. Predictive entropy search for multi-objective bayesian optimization. In *International conference on machine learning*, pages 1492–1501. PMLR, 2016.
- [24] Claus Hillermeier. Nonlinear Multiobjective Optimization: A Generalized Homotopy Approach, volume 135. Springer Science & Business Media, 2001.
- [25] Hisao Ishibuchi, Hiroyuki Masuda, Yuki Tanigaki, and Yusuke Nojima. Modified distance calculation in generational distance and inverted generational distance. In *International conference on evolutionary multi-criterion optimization*, pages 110–125. Springer, 2015.
- [26] Himanshu Jain and Kalyanmoy Deb. An evolutionary many-objective optimization algorithm using reference-point based nondominated sorting approach, part ii: Handling constraints and extending to an adaptive approach. *IEEE Transactions on evolutionary computation*, 18(4): 602–622, 2013.
- [27] Shan Jiang, Hongyan Zhang, Wenfeng Cong, Zhengyuan Liang, Qiran Ren, Chong Wang, Fusuo Zhang, and Xiaoqiang Jiao. Multi-objective optimization of smallholder apple production: Lessons from the bohai bay region. *Sustainability*, 12(16):6496, 2020.
- [28] Faranak Karamian, Ali Asghar Mirakzadeh, and Arash Azari. Application of multi-objective genetic algorithm for optimal combination of resources to achieve sustainable agriculture based on the water-energy-food nexus framework. Science of The Total Environment, 860:160419, 2023.
- [29] Florian Karl, Tobias Pielok, Julia Moosbauer, Florian Pfisterer, Stefan Coors, Martin Binder, Lennart Schneider, Janek Thomas, Jakob Richter, Michel Lang, et al. Multi-objective hyperparameter optimization in machine learning—an overview. *ACM Transactions on Evolutionary Learning and Optimization*, 3(4):1–50, 2023.
- [30] Johannes Kirschner, Manuel Nonnenmacher, Mojmír Mutnỳ, Andreas Krause, Nicole Hiller, Rasmus Ischebeck, and Andreas Adelmann. Bayesian optimisation for fast and safe parameter tuning of swissfel. In *FEL2019, Proceedings of the 39th International Free-Electron Laser Conference*, pages 707–710. JACoW Publishing, 2019.
- [31] Joshua Knowles. Parego: A hybrid algorithm with on-line landscape approximation for expensive multiobjective optimization problems. *IEEE transactions on evolutionary computation*, 10 (1):50–66, 2006.
- [32] Takehisa Kohira, Hiromasa Kemmotsu, Oyama Akira, and Tomoaki Tatsukawa. Proposal of benchmark problem based on real-world car structure design optimization. In *Proceedings of the Genetic and Evolutionary Computation Conference Companion*, pages 183–184, 2018.

- [33] Mina Konakovic Lukovic, Yunsheng Tian, and Wojciech Matusik. Diversity-guided multiobjective bayesian optimization with batch evaluations. *Advances in Neural Information Processing Systems*, 33:17708–17720, 2020.
- [34] Sallam A Kouritem, Mohammed I Abouheaf, Nabil Nahas, and Mohamed Hassan. A multiobjective optimization design of industrial robot arms. *Alexandria Engineering Journal*, 61(12): 12847–12867, 2022.
- [35] Dieter Kraft. A software package for sequential quadratic programming. Forschungsbericht-Deutsche Forschungs- und Versuchsanstalt fur Luft- und Raumfahrt, 1988.
- [36] Xi Lin, Xiaoyuan Zhang, Zhiyuan Yang, Fei Liu, Zhenkun Wang, and Qingfu Zhang. Smooth tchebycheff scalarization for multi-objective optimization. In *International Conference on Machine Learning*, pages 30479–30509. PMLR, 2024.
- [37] Jonas Močkus. On bayesian methods for seeking the extremum. In *Optimization Techniques IFIP Technical Conference Novosibirsk*, July 1–7, 1974 6, pages 400–404. Springer, 1975.
- [38] Sarah Müller, Alexander von Rohr, and Sebastian Trimpe. Local policy search with bayesian optimization. Advances in Neural Information Processing Systems, 34:20708–20720, 2021.
- [39] Hirotaka Nakayama, Yeboon Yun, and Min Yoon. Sequential approximate multiobjective optimization using computational intelligence. Springer Science & Business Media, 2009.
- [40] Lam Ngo, Huong Ha, Jeffrey Chan, and Hongyu Zhang. Boids: High-dimensional bayesian optimization via incumbent-guided direction lines and subspace embeddings. In *Proceedings of the AAAI Conference on Artificial Intelligence*, volume 39, pages 19659–19667, 2025.
- [41] Biswajit Paria, Kirthevasan Kandasamy, and Barnabás Póczos. A flexible framework for multi-objective bayesian optimization using random scalarizations. In *Uncertainty in Artificial Intelligence*, pages 766–776. PMLR, 2020.
- [42] Adam Paszke, Sam Gross, Soumith Chintala, Gregory Chanan, Edward Yang, Zachary DeVito, Zeming Lin, Alban Desmaison, Luca Antiga, and Adam Lerer. Automatic differentiation in pytorch. In *NIPS-W*, 2017.
- [43] Michael JD Powell. A direct search optimization method that models the objective and constraint functions by linear interpolation. Springer, 1994.
- [44] Jixiang Qing, Henry B Moss, Tom Dhaene, and Ivo Couckuyt. Pf2es: Parallel feasible pareto frontier entropy search for multi-objective bayesian optimization. In *International Conference on Artificial Intelligence and Statistics*, pages 2565–2588. PMLR, 2023.
- [45] Nery Riquelme, Christian Von Lücken, and Benjamin Baran. Performance metrics in multiobjective optimization. In 2015 Latin American computing conference (CLEI), pages 1–11. IEEE, 2015.
- [46] Adriana Schulz, Harrison Wang, Eitan Grinspun, Justin Solomon, and Wojciech Matusik. Interactive exploration of design trade-offs. ACM Transactions on Graphics (TOG), 37(4):1–14, 2018.
- [47] Ozan Sener and Vladlen Koltun. Multi-task learning as multi-objective optimization. *Advances in neural information processing systems*, 31, 2018.
- [48] Niranjan Srinivas, Andreas Krause, Sham Kakade, and Matthias Seeger. Gaussian process optimization in the bandit setting: No regret and experimental design. In *Proceedings of the 27th International Conference on Machine Learning*, pages 1015–1022. Omnipress, 2010.
- [49] Shinya Suzuki, Shion Takeno, Tomoyuki Tamura, Kazuki Shitara, and Masayuki Karasuyama. Multi-objective bayesian optimization using pareto-frontier entropy. In *International conference on machine learning*, pages 9279–9288. PMLR, 2020.
- [50] Ryoji Tanabe and Hisao Ishibuchi. An easy-to-use real-world multi-objective optimization problem suite. Applied Soft Computing, 89:106078, 2020.

- [51] William R Thompson. On the likelihood that one unknown probability exceeds another in view of the evidence of two samples. *Biometrika*, 25(3/4):285–294, 1933.
- [52] Ben Tu, Axel Gandy, Nikolas Kantas, and Behrang Shafei. Joint entropy search for multiobjective bayesian optimization. Advances in Neural Information Processing Systems, 35: 9922–9938, 2022.
- [53] David A Van Veldhuizen and Gary B Lamont. Multiobjective evolutionary algorithm test suites. In *Proceedings of the 1999 ACM symposium on Applied computing*, pages 351–357, 1999.
- [54] Changyun Wei, Ze Ji, and Boliang Cai. Particle swarm optimization for cooperative multi-robot task allocation: a multi-objective approach. In *IEEE Robotics and Automation Letters*, volume 5, pages 2530–2537. IEEE, 2020.
- [55] Christopher KI Williams and Carl Edward Rasmussen. *Gaussian processes for machine learning*, volume 2. MIT press Cambridge, MA, 2006.
- [56] Pengcheng Xu, Yingying Ma, Wencong Lu, Minjie Li, Wenyue Zhao, and Zhilong Dai. Multi-objective optimization in machine learning assisted materials design and discovery. *Journal of Materials Informatics*, 5(2):N–A, 2025.
- [57] Qingfu Zhang and Hui Li. Moea/d: A multiobjective evolutionary algorithm based on decomposition. *IEEE Transactions on evolutionary computation*, 11(6):712–731, 2007.
- [58] Richard Zhang and Daniel Golovin. Random hypervolume scalarizations for provable multiobjective black box optimization. In *International conference on machine learning*, pages 11096–11105. PMLR, 2020.
- [59] Eckart Zitzler and Lothar Thiele. Multiobjective evolutionary algorithms: a comparative case study and the strength pareto approach. *IEEE transactions on Evolutionary Computation*, 3(4): 257–271, 2002.
- [60] Eckart Zitzler, Lothar Thiele, Marco Laumanns, Carlos M Fonseca, and Viviane Grunert Da Fonseca. Performance assessment of multiobjective optimizers: An analysis and review. *IEEE Transactions on evolutionary computation*, 7(2):117–132, 2003.
- [61] Marcela Zuluaga, Guillaume Sergent, Andreas Krause, and Markus Püschel. Active learning for multi-objective optimization. In *International conference on machine learning*, pages 462–470. PMLR, 2013.

NeurIPS Paper Checklist

1. Claims

Question: Do the main claims made in the abstract and introduction accurately reflect the paper's contributions and scope?

Answer: [Yes]

Justification: We propose a multi-objective Bayesian Optimization algorithm, which can outperform the state-of-the-art methods. We provide experiments and analysis to support our claim.

Guidelines:

- The answer NA means that the abstract and introduction do not include the claims made in the paper.
- The abstract and/or introduction should clearly state the claims made, including the
 contributions made in the paper and important assumptions and limitations. A No or
 NA answer to this question will not be perceived well by the reviewers.
- The claims made should match theoretical and experimental results, and reflect how much the results can be expected to generalize to other settings.
- It is fine to include aspirational goals as motivation as long as it is clear that these goals are not attained by the paper.

2. Limitations

Question: Does the paper discuss the limitations of the work performed by the authors?

Answer: [Yes]

Justification: We provide the limitation in the Conclusion section (Sec. 6)

Guidelines:

- The answer NA means that the paper has no limitation while the answer No means that the paper has limitations, but those are not discussed in the paper.
- The authors are encouraged to create a separate "Limitations" section in their paper.
- The paper should point out any strong assumptions and how robust the results are to violations of these assumptions (e.g., independence assumptions, noiseless settings, model well-specification, asymptotic approximations only holding locally). The authors should reflect on how these assumptions might be violated in practice and what the implications would be.
- The authors should reflect on the scope of the claims made, e.g., if the approach was only tested on a few datasets or with a few runs. In general, empirical results often depend on implicit assumptions, which should be articulated.
- The authors should reflect on the factors that influence the performance of the approach. For example, a facial recognition algorithm may perform poorly when image resolution is low or images are taken in low lighting. Or a speech-to-text system might not be used reliably to provide closed captions for online lectures because it fails to handle technical jargon.
- The authors should discuss the computational efficiency of the proposed algorithms and how they scale with dataset size.
- If applicable, the authors should discuss possible limitations of their approach to address problems of privacy and fairness.
- While the authors might fear that complete honesty about limitations might be used by reviewers as grounds for rejection, a worse outcome might be that reviewers discover limitations that aren't acknowledged in the paper. The authors should use their best judgment and recognize that individual actions in favor of transparency play an important role in developing norms that preserve the integrity of the community. Reviewers will be specifically instructed to not penalize honesty concerning limitations.

3. Theory assumptions and proofs

Question: For each theoretical result, does the paper provide the full set of assumptions and a complete (and correct) proof?

Answer: [NA]

Justification: There is no theoretical result.

Guidelines:

- The answer NA means that the paper does not include theoretical results.
- All the theorems, formulas, and proofs in the paper should be numbered and cross-referenced.
- All assumptions should be clearly stated or referenced in the statement of any theorems.
- The proofs can either appear in the main paper or the supplemental material, but if they appear in the supplemental material, the authors are encouraged to provide a short proof sketch to provide intuition.
- Inversely, any informal proof provided in the core of the paper should be complemented by formal proofs provided in appendix or supplemental material.
- Theorems and Lemmas that the proof relies upon should be properly referenced.

4. Experimental result reproducibility

Question: Does the paper fully disclose all the information needed to reproduce the main experimental results of the paper to the extent that it affects the main claims and/or conclusions of the paper (regardless of whether the code and data are provided or not)?

Answer: [Yes]

Justification: We provide the settings for our proposed method and baselines in the Appendix A.7.

Guidelines:

- The answer NA means that the paper does not include experiments.
- If the paper includes experiments, a No answer to this question will not be perceived well by the reviewers: Making the paper reproducible is important, regardless of whether the code and data are provided or not.
- If the contribution is a dataset and/or model, the authors should describe the steps taken to make their results reproducible or verifiable.
- Depending on the contribution, reproducibility can be accomplished in various ways. For example, if the contribution is a novel architecture, describing the architecture fully might suffice, or if the contribution is a specific model and empirical evaluation, it may be necessary to either make it possible for others to replicate the model with the same dataset, or provide access to the model. In general, releasing code and data is often one good way to accomplish this, but reproducibility can also be provided via detailed instructions for how to replicate the results, access to a hosted model (e.g., in the case of a large language model), releasing of a model checkpoint, or other means that are appropriate to the research performed.
- While NeurIPS does not require releasing code, the conference does require all submissions to provide some reasonable avenue for reproducibility, which may depend on the nature of the contribution. For example
 - (a) If the contribution is primarily a new algorithm, the paper should make it clear how to reproduce that algorithm.
- (b) If the contribution is primarily a new model architecture, the paper should describe the architecture clearly and fully.
- (c) If the contribution is a new model (e.g., a large language model), then there should either be a way to access this model for reproducing the results or a way to reproduce the model (e.g., with an open-source dataset or instructions for how to construct the dataset).
- (d) We recognize that reproducibility may be tricky in some cases, in which case authors are welcome to describe the particular way they provide for reproducibility. In the case of closed-source models, it may be that access to the model is limited in some way (e.g., to registered users), but it should be possible for other researchers to have some path to reproducing or verifying the results.

5. Open access to data and code

Question: Does the paper provide open access to the data and code, with sufficient instructions to faithfully reproduce the main experimental results, as described in supplemental material?

Answer: [Yes]

Justification: We provide the code in the supplementary materials. We will also make the code public after acceptance.

Guidelines:

- The answer NA means that paper does not include experiments requiring code.
- Please see the NeurIPS code and data submission guidelines (https://nips.cc/public/guides/CodeSubmissionPolicy) for more details.
- While we encourage the release of code and data, we understand that this might not be possible, so "No" is an acceptable answer. Papers cannot be rejected simply for not including code, unless this is central to the contribution (e.g., for a new open-source benchmark).
- The instructions should contain the exact command and environment needed to run to reproduce the results. See the NeurIPS code and data submission guidelines (https://nips.cc/public/guides/CodeSubmissionPolicy) for more details.
- The authors should provide instructions on data access and preparation, including how
 to access the raw data, preprocessed data, intermediate data, and generated data, etc.
- The authors should provide scripts to reproduce all experimental results for the new proposed method and baselines. If only a subset of experiments are reproducible, they should state which ones are omitted from the script and why.
- At submission time, to preserve anonymity, the authors should release anonymized versions (if applicable).
- Providing as much information as possible in supplemental material (appended to the paper) is recommended, but including URLs to data and code is permitted.

6. Experimental setting/details

Question: Does the paper specify all the training and test details (e.g., data splits, hyperparameters, how they were chosen, type of optimizer, etc.) necessary to understand the results?

Answer: [Yes]

Justification: The experiment settings, including the hyperparamters for the methods and the details of benchmark functions are presented in Sec. 5 and Appendix A.6.

Guidelines:

- The answer NA means that the paper does not include experiments.
- The experimental setting should be presented in the core of the paper to a level of detail that is necessary to appreciate the results and make sense of them.
- The full details can be provided either with the code, in appendix, or as supplemental material.

7. Experiment statistical significance

Question: Does the paper report error bars suitably and correctly defined or other appropriate information about the statistical significance of the experiments?

Answer: [Yes]

Justification: In all our experiments, we provide the error bar to represent the randomness of the experiments.

- The answer NA means that the paper does not include experiments.
- The authors should answer "Yes" if the results are accompanied by error bars, confidence intervals, or statistical significance tests, at least for the experiments that support the main claims of the paper.

- The factors of variability that the error bars are capturing should be clearly stated (for example, train/test split, initialization, random drawing of some parameter, or overall run with given experimental conditions).
- The method for calculating the error bars should be explained (closed form formula, call to a library function, bootstrap, etc.)
- The assumptions made should be given (e.g., Normally distributed errors).
- It should be clear whether the error bar is the standard deviation or the standard error
 of the mean.
- It is OK to report 1-sigma error bars, but one should state it. The authors should preferably report a 2-sigma error bar than state that they have a 96% CI, if the hypothesis of Normality of errors is not verified.
- For asymmetric distributions, the authors should be careful not to show in tables or figures symmetric error bars that would yield results that are out of range (e.g. negative error rates).
- If error bars are reported in tables or plots, The authors should explain in the text how they were calculated and reference the corresponding figures or tables in the text.

8. Experiments compute resources

Question: For each experiment, does the paper provide sufficient information on the computer resources (type of compute workers, memory, time of execution) needed to reproduce the experiments?

Answer: [Yes]

Justification: We present the computing resources used for all experiments in the Appendix A.10.

Guidelines:

- The answer NA means that the paper does not include experiments.
- The paper should indicate the type of compute workers CPU or GPU, internal cluster, or cloud provider, including relevant memory and storage.
- The paper should provide the amount of compute required for each of the individual experimental runs as well as estimate the total compute.
- The paper should disclose whether the full research project required more compute than the experiments reported in the paper (e.g., preliminary or failed experiments that didn't make it into the paper).

9. Code of ethics

Question: Does the research conducted in the paper conform, in every respect, with the NeurIPS Code of Ethics https://neurips.cc/public/EthicsGuidelines?

Answer: [Yes]

Justification: Our work comply with the NeurIPS Code of Ethics.

Guidelines:

- The answer NA means that the authors have not reviewed the NeurIPS Code of Ethics.
- If the authors answer No, they should explain the special circumstances that require a deviation from the Code of Ethics.
- The authors should make sure to preserve anonymity (e.g., if there is a special consideration due to laws or regulations in their jurisdiction).

10. Broader impacts

Question: Does the paper discuss both potential positive societal impacts and negative societal impacts of the work performed?

Answer: [NA]

Justification: This paper propose an optimization algorithm. There should be no direct societal impacts that must be specifically highlighted here.

Guidelines:

• The answer NA means that there is no societal impact of the work performed.

- If the authors answer NA or No, they should explain why their work has no societal impact or why the paper does not address societal impact.
- Examples of negative societal impacts include potential malicious or unintended uses (e.g., disinformation, generating fake profiles, surveillance), fairness considerations (e.g., deployment of technologies that could make decisions that unfairly impact specific groups), privacy considerations, and security considerations.
- The conference expects that many papers will be foundational research and not tied to particular applications, let alone deployments. However, if there is a direct path to any negative applications, the authors should point it out. For example, it is legitimate to point out that an improvement in the quality of generative models could be used to generate deepfakes for disinformation. On the other hand, it is not needed to point out that a generic algorithm for optimizing neural networks could enable people to train models that generate Deepfakes faster.
- The authors should consider possible harms that could arise when the technology is being used as intended and functioning correctly, harms that could arise when the technology is being used as intended but gives incorrect results, and harms following from (intentional or unintentional) misuse of the technology.
- If there are negative societal impacts, the authors could also discuss possible mitigation strategies (e.g., gated release of models, providing defenses in addition to attacks, mechanisms for monitoring misuse, mechanisms to monitor how a system learns from feedback over time, improving the efficiency and accessibility of ML).

11. Safeguards

Question: Does the paper describe safeguards that have been put in place for responsible release of data or models that have a high risk for misuse (e.g., pretrained language models, image generators, or scraped datasets)?

Answer: [NA]

Justification: We believe our work does not pose any risk.

Guidelines:

- The answer NA means that the paper poses no such risks.
- Released models that have a high risk for misuse or dual-use should be released with necessary safeguards to allow for controlled use of the model, for example by requiring that users adhere to usage guidelines or restrictions to access the model or implementing safety filters.
- Datasets that have been scraped from the Internet could pose safety risks. The authors should describe how they avoided releasing unsafe images.
- We recognize that providing effective safeguards is challenging, and many papers do not require this, but we encourage authors to take this into account and make a best faith effort.

12. Licenses for existing assets

Question: Are the creators or original owners of assets (e.g., code, data, models), used in the paper, properly credited and are the license and terms of use explicitly mentioned and properly respected?

Answer: [Yes]

Justification: All the baseline implementation are open access. All the real-world benchmark problems are also open access.

- The answer NA means that the paper does not use existing assets.
- The authors should cite the original paper that produced the code package or dataset.
- The authors should state which version of the asset is used and, if possible, include a URL.
- The name of the license (e.g., CC-BY 4.0) should be included for each asset.
- For scraped data from a particular source (e.g., website), the copyright and terms of service of that source should be provided.

- If assets are released, the license, copyright information, and terms of use in the
 package should be provided. For popular datasets, paperswithcode.com/datasets
 has curated licenses for some datasets. Their licensing guide can help determine the
 license of a dataset.
- For existing datasets that are re-packaged, both the original license and the license of the derived asset (if it has changed) should be provided.
- If this information is not available online, the authors are encouraged to reach out to the asset's creators.

13. New assets

Question: Are new assets introduced in the paper well documented and is the documentation provided alongside the assets?

Answer: [NA]

Justification: The paper does not release new asset.

Guidelines:

- The answer NA means that the paper does not release new assets.
- Researchers should communicate the details of the dataset/code/model as part of their submissions via structured templates. This includes details about training, license, limitations, etc.
- The paper should discuss whether and how consent was obtained from people whose asset is used.
- At submission time, remember to anonymize your assets (if applicable). You can either create an anonymized URL or include an anonymized zip file.

14. Crowdsourcing and research with human subjects

Question: For crowdsourcing experiments and research with human subjects, does the paper include the full text of instructions given to participants and screenshots, if applicable, as well as details about compensation (if any)?

Answer: [NA]

Justification: Our work does not involve crowdsourcing or research with human subjects.

Guidelines:

- The answer NA means that the paper does not involve crowdsourcing nor research with human subjects.
- Including this information in the supplemental material is fine, but if the main contribution of the paper involves human subjects, then as much detail as possible should be included in the main paper.
- According to the NeurIPS Code of Ethics, workers involved in data collection, curation, or other labor should be paid at least the minimum wage in the country of the data collector.

15. Institutional review board (IRB) approvals or equivalent for research with human subjects

Question: Does the paper describe potential risks incurred by study participants, whether such risks were disclosed to the subjects, and whether Institutional Review Board (IRB) approvals (or an equivalent approval/review based on the requirements of your country or institution) were obtained?

Answer: [NA]

Justification: The paper does not pose any risks.

- The answer NA means that the paper does not involve crowdsourcing nor research with human subjects.
- Depending on the country in which research is conducted, IRB approval (or equivalent) may be required for any human subjects research. If you obtained IRB approval, you should clearly state this in the paper.

- We recognize that the procedures for this may vary significantly between institutions and locations, and we expect authors to adhere to the NeurIPS Code of Ethics and the guidelines for their institution.
- For initial submissions, do not include any information that would break anonymity (if applicable), such as the institution conducting the review.

16. Declaration of LLM usage

Question: Does the paper describe the usage of LLMs if it is an important, original, or non-standard component of the core methods in this research? Note that if the LLM is used only for writing, editing, or formatting purposes and does not impact the core methodology, scientific rigorousness, or originality of the research, declaration is not required.

Answer: [NA]

Justification: The core method development in this research does not involve LLMs as any important, original, or non-standard components.

- The answer NA means that the core method development in this research does not involve LLMs as any important, original, or non-standard components.
- Please refer to our LLM policy (https://neurips.cc/Conferences/2025/LLM) for what should or should not be described.

A Technical Appendices and Supplementary Material

A.1 Normal Boundary Intersection

In this section, we provide more details on the Normal Boundary Intersection (NBI) [11] method, which is a general MOO technique that aims to generate a uniformly distributed set of Pareto optimal solutions. The key insight of the NBI method is that, given a MOO problem, the intersection points between the boundary of the objective space and the vectors orthogonal to the convex hull of individual minima (CHIM) of the objectives could be Pareto optimal solutions. Given the MOO problem in Eq. (1), the NBI method first determines the individual optima of each objective $\mathbf{f}_m^* = \mathbf{f}(\mathbf{x}_m^*)$ where $\mathbf{x}_m^* = \underset{\mathbf{x} \in \mathcal{X}}{\operatorname{argmin}}_{\mathbf{x} \in \mathcal{X}} f_m(\mathbf{x})$ for $m = 1, \dots, M$. Denote a column matrix $\mathbf{F}^* = [\mathbf{f}_1^*, \mathbf{f}_2^*, \dots, \mathbf{f}_M^*]^{\mathsf{T}}$, the CHIM is constructed by a set of points $\{\mathcal{U}(\boldsymbol{\beta})\}$ such that $\mathcal{U}(\boldsymbol{\beta}) = \{\mathbf{F}^*\boldsymbol{\beta} = \sum_{i=1}^M \beta_i \mathbf{f}_i \mid \boldsymbol{\beta} \in \mathbb{R}^M, \sum_{i=1}^M \beta_i \mathbf{f}_i \mid \boldsymbol{\beta} \in \mathbb{R}^M, \sum_{i=1}^M \beta_i \mathbf{f}_i \mid \boldsymbol{\beta} \in \mathbb{R}^M$, where $\boldsymbol{\beta} = [\beta_1, \dots, \beta_M]$ is a convex combination weight vector to construct points on CHIM. For each point $\mathcal{U}(\beta)$, NBI defines a constrained optimization problem, referred to as the NBI subproblems, along the direction normal to CHIM, i.e., $(\mathbf{x}^*, \lambda^*) \in \max_{\lambda \in \mathbb{R}, \mathbf{x} \in \mathcal{X}} \lambda$ subject to $\mathcal{U}(\beta) + \lambda \mathbf{n} = \mathbf{f}(\mathbf{x})$, where **n** is the normal vector of CHIM. Solving this constrained optimization problem results in a data point x^* corresponding to the intersection point $f(x^*)$ that is expected to be Pareto optimal. As a result, by solving multiple NBI subproblems defined over a set of welldistributed points $\mathcal{U}(\beta)$ on the CHIM, the NBI method is expected to result in a set of well-distributed n_{β} Pareto optimal solutions for the MOO problem in Eq. (1). The geometric intuition ensures uniform spacing of solutions and is particularly suitable for problems with complex, non-convex Pareto fronts. However, solving the NBI problem requires evaluating the objective functions f(x)for the constraint term, which is impractical for expensive objective functions and limited evaluation budget as in MOBO.

In NBI, the set of well-distributed $\beta = [\beta_1, \dots, \beta_M]$ is constructed using a structured approach as follows. Given an integer number denoting the number of partition n_p , possible values for each β_i are $\{0, \delta, 2\delta, \dots, 1\}$ where $\delta = 1/n_p$ is the step-size. Then, we sequentially select each β_i such that they satisfy $\sum_{i=1}^M \beta_i = 1$. In practice, the possible values for β_j corresponding to $\beta_i = m_i \delta$ for $i = 1, \dots, j-1$ and $j = 2, \dots, M-1$ are $\left\{0, \delta, 2\delta, \dots, (p-\sum_{i=1}^{j-1} m_i)\delta\right\}$. Because of this formulation, the number of convex combination weight vectors $\boldsymbol{\beta}$ (and the number of points on CHIM $\mathcal{U}(\boldsymbol{\beta})$) is determined via the binominal coefficients as $n_{\beta} = \binom{M+p-1}{p}$. As a result, this structured formulation cannot generate any arbitrary number of n_{β} , as it ultimately depends on the number of partitions p instead. Our proposed MOBO-OSD algorithm leverages a different point generation method (Sec 4.1) that can handle any arbitrary number of n_{β} , while maintaining the desired well-distributed property.

A.2 Pareto Front Estimation via First Order Approximation

This section summarizes the First Order Approximation technique [46] to estimate the Pareto front of a MO problem. In MOO, discovering the entire Pareto front \mathcal{P}_f can be challenging, however, once we find a Pareto optimal solution $\mathbf{x}^* \in \mathcal{P}_f$, it is easier to find nearby Pareto optimal solutions by locally exploring around \mathbf{x}^* [46, 33]. Pareto Front First Order Approximation technique [46] leverages this fact to approximate the Pareto front from a previously discovered Pareto optimal solution. Given the MOO problem in Eq. (1) and an observed Pareto optimal input \mathbf{x}^* found so far, the key idea is to construct a local exploration space $\mathcal{T} \subset \mathcal{X}$ around \mathbf{x}^* . In particular, \mathcal{T} is a linear combination of a set of exploration vectors \mathbf{v} which are obtained by solving the following equation:

$$\begin{cases}
\mathbf{H}\mathbf{v} \in \operatorname{Im}\left(\mathcal{J}_{F}(\mathbf{x}^{*})\right) \oplus \operatorname{Im}\left(\mathcal{J}_{G}(\mathbf{x}^{*})\right), \\
\mathcal{J}_{G}^{\mathsf{T}}(\mathbf{x}^{*})\mathbf{v} = 0,
\end{cases} (5)$$

where $\mathbf{H} = \sum_{i=1}^{M} \alpha_i \mathcal{H}_{f_i}(\mathbf{x}^*) + \sum_{k=1}^{K} \beta_k \mathcal{H}_{g_k}(\mathbf{x}^*)$ corresponds to the derivatives of the stationarity KTT condition; \mathcal{J}_F and \mathcal{J}_G are the Jacobian matrix of all objectives \mathbf{f} and K active constraints \mathbf{g} , respectively; \mathcal{H}_u is the Hessian matrix of an arbitrary function u and $\alpha = [\alpha_1, \ldots, \alpha_M]$ and $\beta = [\beta_1, \ldots, \beta_K]$ are the Lagrange multipliers (dual variables) associated with the KKT conditions [24] of the MOO problem in Eq. (1). The first equation in Eq. (5) ensures that moving \mathbf{x}^* along direction \mathbf{v} still preserves the stationarity KKT conditions, ensuring the Pareto optimality of the resulting solutions. Additionally, the second equation ensures the feasibility of active constraints \mathbf{g} that appear when \mathbf{x}^* is very close to a boundary of \mathcal{X} . Overall, this technique can help to discover more

solutions nearby the current Pareto optimal solution $f(\mathbf{x}^*)$. Schulz et al. [46] shows that, generally, $\dim(\mathcal{T}) = \min(M-1,D)$. Having the local exploration space \mathcal{T} with exploration vectors \mathbf{v} , we can generate additional Pareto optimal solutions around the previously discovered Pareto optimal solutions \mathbf{x}^* .

A.3 Details on the Proposed Orthogonal Search Directions

This section presents the details when computing the normal direction of the approximated CHIM (Sec. 4.1). In MOBO-OSD, following Das and Dennis [11], instead of using the exact normal direction $\bar{\mathbf{n}}$ where $\mathbf{P}\bar{\mathbf{n}}^{\mathsf{T}}=\mathbf{0}$, we employ quasi-normal directions for consistent scaling across all objectives, preventing potential ill-conditioning. Specifically, the proposed orthogonal search direction $\hat{\mathbf{n}}$ for MOBO-OSD is defined as $\hat{\mathbf{n}}=-\mathbf{P}e$ where e is a column vector of all ones. The formula computes an equally weighted linear combination of the boundary points \mathbf{p}_m , then multiplied by -1 to ensure the normal vector points to the origin. Then we normalize normal vector to unit length $\mathbf{n}=\hat{\mathbf{n}}/\|\hat{\mathbf{n}}\|$. The quasi-normal direction can be interpreted as applying a normalization to remove the difference in scaling among the objectives, while maintaining similar results of subproblems, i.e., the intersection points found.

A.4 Advantages of OSD Subproblems Compared to Other Scalarization Techniques

In this section, we provide a discussion on the advantages of our propose OSD subproblem formulation compared to the most closely related scalarization technique - linear scalarization (LS) [41]. First, LS generates search directions at random, which can be less efficient than the data-driven search directions proposed in our OSD formulation. Second, even when LS weight vectors are welldistributed (e.g., using Riesz s-Energy [8]), LS is limited to finding solutions on the convex regions of the Pareto front [58]. In contrast, our proposed OSD formulation is capable of identifying solutions on the Pareto front of arbitrary shape, including both convex and non-convex regions. Note that due to this limitation, LS has been superseded by the most widely used scalarization technique - Tchebychev scalarization (TCH) [41]. TCH can handle non-convex PF and has been widely selected in other works when evaluating scalarization techniques [41, 31, 13, 33]. However, one critical drawback of TCH lies in its non-smooth formulation caused by the maximization operator, which makes TCH suffers from non-differentiability and slow convergence [36]. On the other hand, the MOBO-OSD subproblem formulation is differentiable, either analytically under common kernels or by automatic differentiation via computational graphs, as described in Sec. 4.2. Empirically, our proposed method consistently outperforms baselines employing TCH, such as qParEGO. Figures 2, 3, 5 and 6 show that MOBO-OSD outperforms qParEGO across different benchmark functions with diverse PF characteristics, including convex (ZDT1) and concave (DTLZ2).

A.5 Comparison To Other Line-based BO Algorithms

As our proposed MOBO-OSD algorithm conducts search for Pareto optimal solution along *one-dimensional guiding lines*, in this section, we discuss the key differences compared to other recent line-based BO algorithms, such as LineBO [30] and BOIDS [40]. The primary distinction lies in the formulation of these one-dimensional lines: both LineBO and BOIDS construct search directions with some degree of *randomness*, whereas MOBO-OSD relies on *deterministic* OSD directions that are orthogonal to the approximated CHIM. Additionally, another key difference is in the search domain: LineBO and BOIDS define one-dimensional lines in the *input space*, while our MOBO-OSD formulates one-dimensional search directions in the *output space*. Furthermore, LineBO and BOIDS are primarily *designed to make high-dimensional problems tractable*, while MOBO-OSD focuses on *generating a well-distributed set of Pareto optimal points* on the Pareto front. Therefore, LineBO and BOIDS are fundamentally different approaches and are not compatible with the MOBO settings. In contrast, MOBO-OSD is specifically designed for MOBO problems, with the core purpose of generating orthogonal search directions relative to the approximated CHIM to ensure a well-distributed coverage of the Pareto front.

A.6 Details of Benchmark Problems

We present the details of all benchmark problems in Table 2. The reference points for synthetic problems are similar to many MOBO works [13, 14, 1]. To compute the reference point for real-world

problems, we follow a common rule [13, 33, 50] and generate a pool of observed data points to compute the reference point via the pool's nadir and ideal points as $\mathbf{r} = \mathbf{y}^{\text{nadir}} + 0.1 * (\mathbf{y}^{\text{nadir}} - \mathbf{y}^{\text{ideal}})$. All baselines use similar reference points both when running the code implementation (if required) and when computing the hypervolume difference as comparison metric.

Table 2: Details of 5 synthetic (ZDT1, VLMOP2, DTLZ2-M2, DTLZ2-M3, DTLZ2-M4) and 4 real-world (Speed Reducer, Car Side Design, Marine Design, Water Planning) benchmark problems.

Problem	D	M	Reference Point
DTLZ2-M2	5	2	(1.1, 1.1)
DTLZ2-M3	5	3	(1.1, 1.1, 1.1)
DTLZ2-M4	5	4	(1.1, 1.1, 1.1, 1.1)
ZDT1	5	2	(11.0, 11.0)
VLMOP2	5	2	(1.0, 1.0)
Speed Reducer	7	3	(6735.9, 1761.17, 402.34)
Car Side Design	7	4	(38.89, 4.44, 12.94, 8.87)
Marine Design	6	4	(-210.44, 18970.82, 24111.07, 11.36)
Water Planning	3	6	(84349, 1461, 3101484, 12442800, 67030, 1.59)

A.7 Detailed Implementation

We implemented MOBO-OSD and all baselines in Python (version 3.10). The detailed implementation are as follows.

MOBO-OSD. For the surrogate model, we implement the GPs via GPyTorch [20] and BoTorch [3]. We follow [33] and use Matérn 5/2 kernel with the ARD length-scales in the interval $\sqrt{10^{-3}}$, $\sqrt{10^3}$ and signal variance in the interval $\sqrt{10^{-3}}$, $\sqrt{10^3}$. The Gaussian likelihood is modeled with standard homoskedastic noise in the interval $[10^{-6}, 10^{-3}]$.

For the number of points on approximated CHIM, we set the default value $n_{\beta}=20$ and present an ablation study of other settings in Sec. 5.2. For the scaling of confidence region, we use the common 95% confidence interval, i.e., $\delta=1.96$ [21]. For the number of starting points when solving MOBO-OSD subproblem, we set $n_s=4$. Our code implementation can be found at https://github.com/LamNgo1/mobo-osd.

PDBO [1]. We use the default hyperparameter settings from the paper, including the Hedge algorithm for selecting acquisition functions, the pool of acquisition functions EI, UCB, TS and Identity (i.e., the posterior mean function). We use the open-sourced implementation at https://github.com/Alaleh/PDBO.

qEHVI [13]. We use the default hyperparameter settings from the paper. This includes the batch selection strategy that use sequential greedy approach to integrate over the unobserved outcomes. We use the open-sourced implementation at https://github.com/pytorch/botorch.

DGEMO [33]. We use the default hyperparameter settings from the paper, including the number of buffer cells, max number of samples in each cell, buffer origin, graph-cut hyperparameters and solver NSGA-II hyperparameters. We use the open-sourced implementation at https://github.com/yunshengtian/DGEMO.

USeMO [5]. We use the default hyperparameter settings from the paper. For the acquisition function, we use the EI [37] as it has the overall best performance and is widely compared in other works. We use the open-sourced implementation at https://github.com/belakaria/USeMO.

qParEGO [31]. qParEGO is a novel extension from ParEGO [31] that is developed by Daulton et al. [13] to leverage batch setting. We use the settings as follows: augmented Tchebychev scalarization [39], EI acquisition function with gradient solver and sequential greedy batch selection strategy. We use the open-sourced implementation at https://botorch.org/docs/tutorials.

JES [52]. We use the default hyperparameter settings from the paper. This includes the number of random initialization points for optimizing JES, and the NSGA-II hyperparameter settings for solving the Pareto front. We use the open-sourced implementation at https://github.com/benmltu/JES.

NSGA-II [16]. We use NSGA-II implementation from pymoo [7]. We use the default settings as follows: population size of 100, binary tournament selection, simulated binary crossover (probability p=0.9, exponential distribution parameter $\eta=15$) and polynomial mutation (probability p=0.9, exponential distribution parameter $\eta=20$). We use the open-sourced implementation at https://pymoo.org/algorithms/moo/nsga2.html.

NBI [11]. To the best of our knowledge, there is no available open-source implementation for NBI, therefore we recreated the implementation based on [11] as follows. At first, we sequentially optimize each objective f_m to obtain the individual minima. Then the convex hull of individual minima (CHIM) can be computed via the convex combination weight vectors $\boldsymbol{\beta}$. We use the same Riesz s-Energy method [8] as in MOBO-OSD to generate exact $n_{\beta}=20$ combination weight vectors, since the default point generation strategy cannot work with arbitrary n_{β} . See Appendix A.1 for details. Then, for each of n_{β} NBI subproblems defined at each point on the CHIM, we solve the NBI subproblem to compute the intersections between the CHIM and the NBI normal search directions. Until the evaluation budget depletes, we solve n_{β} NBI subproblems again (with new random initialization) to obtain new solutions. We aggregate all observations found, including when optimizing for the individual minima, when optimizing NBI subproblems and when evaluating the NBI subproblem constraints. Finally, from the observed dataset, we construct the approximate Pareto front for hypervolume comparison against other baselines.

As NBI requires evaluating objective functions for the constraints, the method is not sample-efficient. In fact, in our experiments, NBI often depletes the budget even when not having finished the first round of n_{β} subproblems. We illustrate this statistics by presenting the number of function evaluations required to complete the individual minimum optimization and the first round of n_{β} NBI subproblems given two types of solver, gradient-based SQLSP [35] and gradient-free COBYLA [43]). Details are shown in Table 3. We also present the performance of NBI given these two solvers in Fig. 9.

A.8 Additional Results for Baseline Comparison

On top of the comparison results between MOBO-OSD and the baselines shown in Sec. 5.1, we provide extra results for other batch settings $b = \{8, 10\}$, which are shown in Figs 5 and 6, respectively. Note that qEVHI has limited iterations due to the prohibitively high computational cost (exceeding 12 hours runtime) and memory required (exceeding 64 GB) on problems with $M \geq 4$ objectives and batch size $b = \{8, 10\}$. MOBO-OSD and other baselines can finish the experiments within the given similar resources.

A.9 Additional Results for Ablation Study

Figs 7 and 8 present the full results of the ablation study on n_{β} parameter on all benchmark problems, on both sequential and batch settings, respectively. Overall, all variants have relatively similar performance, indicating the robustness of MOBO-OSD with respect to n_{β} parameter.

A.10 Computing Infrastructure

We run experiments on a computing server with a Dual CPU of type AMD EPYC 7662 (total of 128 Threads, 256 CPUs). Each experiment is allocated 8 CPUs and 64GB Memory. The server is installed with Ubuntu (20.04.3 LTS) Operating System.

A.11 Computational Complexity

We provide the theoretical computational complexity analysis as follows. Let N and n denote the number of surrogate model training and testing points, respectively, and let D and M denote the number of dimensions and objectives, respectively. The computational complexity for the approximated CHIM and OSD formulation is $\mathcal{O}(NM)$ as these steps require iterating over N data points with M-dimensional output. The GP training cost is well-known to scale cubically with the

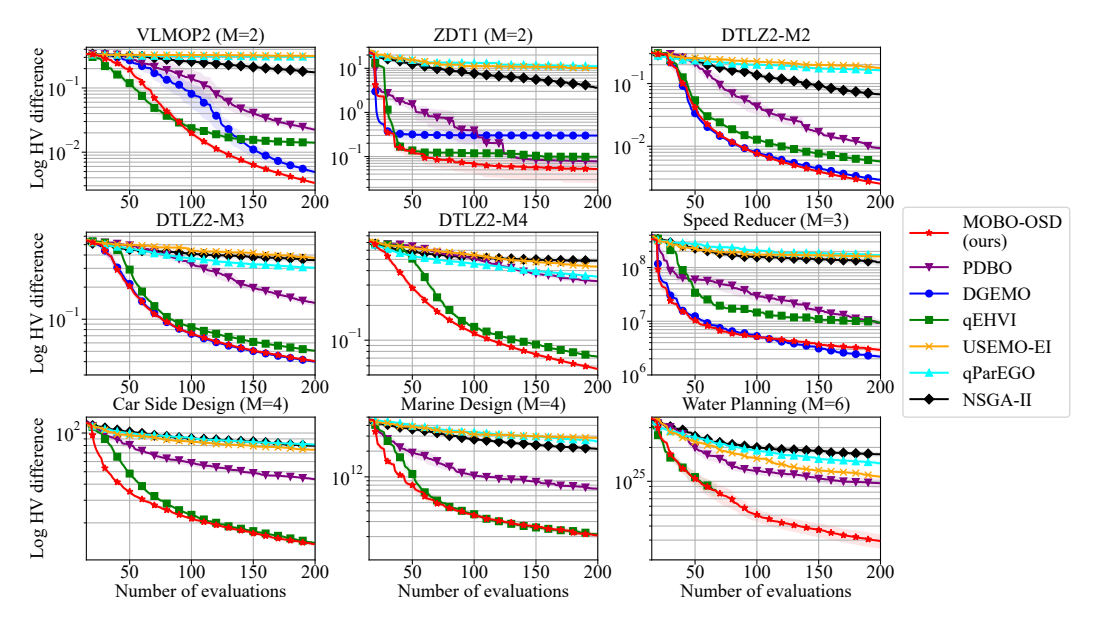


Figure 5: Comparison of MOBO-OSD against the SOTA baselines on 5 synthetic and 4 real-world benchmark problems in batch setting (batch size 8). Note that qEVHI has limited iterations due to the prohibitively high computational cost and memory required on problems with $M \ge 4$ objectives.

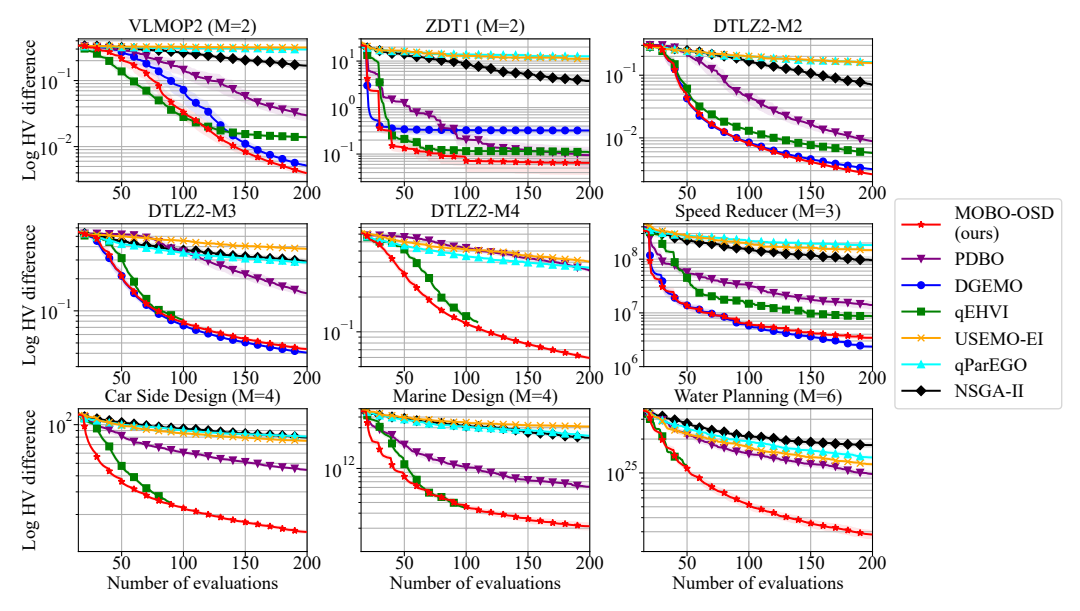


Figure 6: Comparison of MOBO-OSD against the SOTA baselines on 5 synthetic and 4 real-world benchmark problems in batch setting (batch size 10). Note that qEVHI has limited iterations due to the prohibitively high computational cost and memory required on problems with $M \ge 4$ objectives.

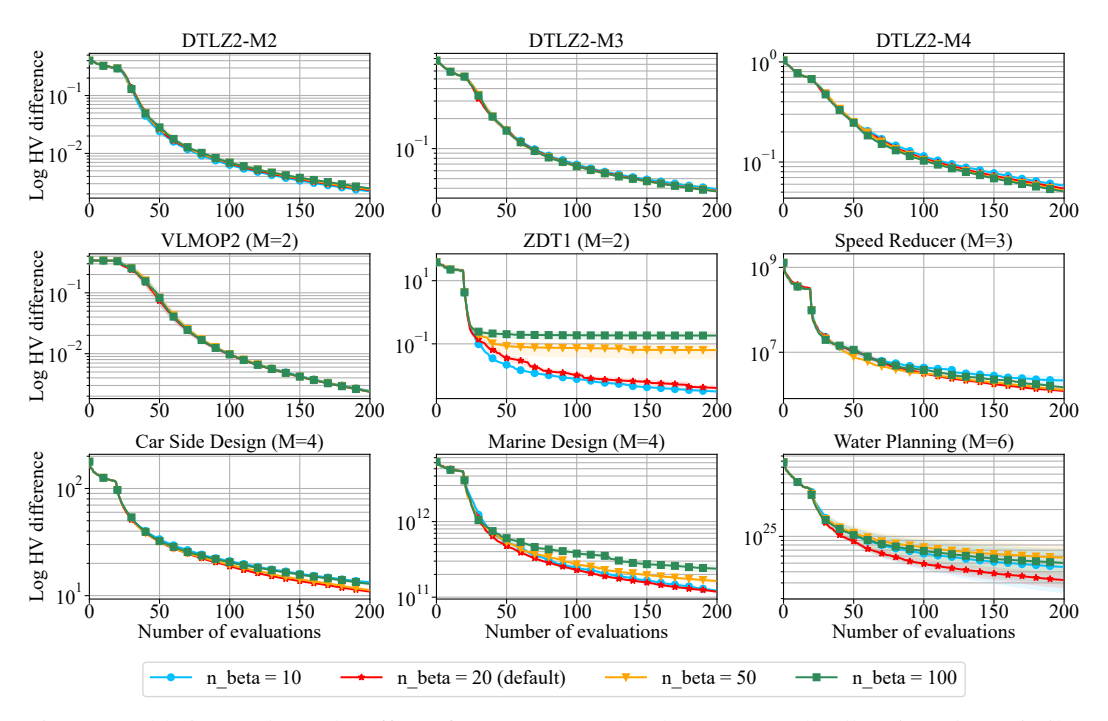


Figure 7: Ablation study on the effect of n_{β} parameter (batch = 1). Overall, all variants have similar performance, indicating the robustness of MOBO-OSD with respect to n_{β} parameter.

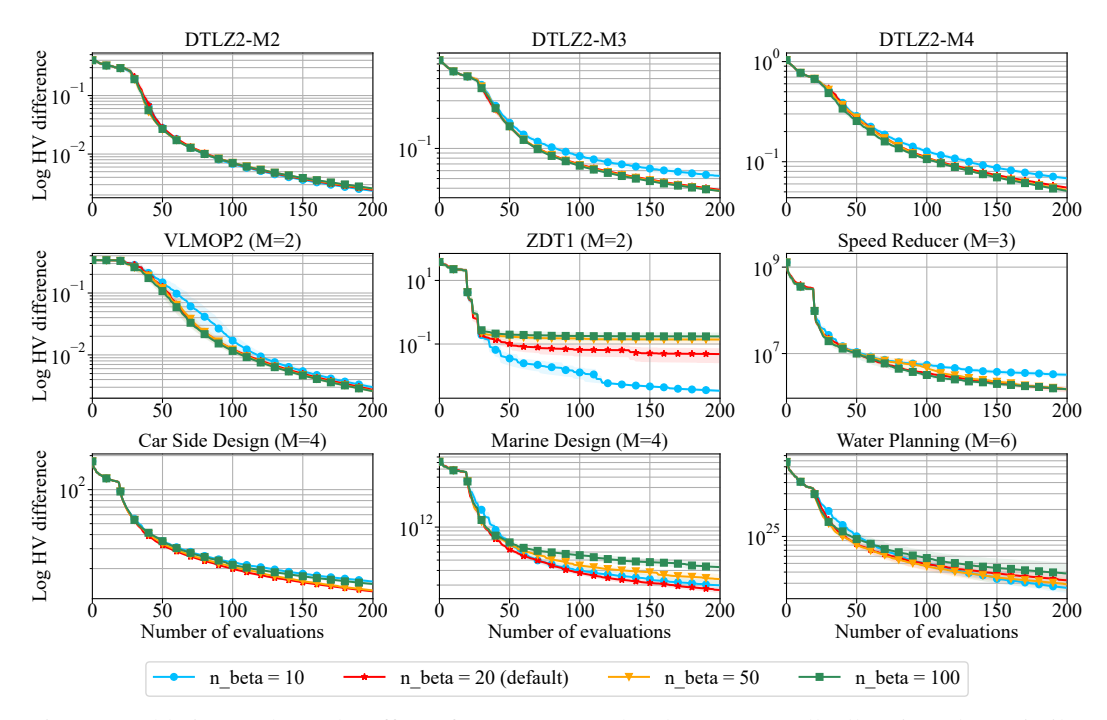


Figure 8: Ablation study on the effect of n_{β} parameter (batch = 4). Overall, all variants have similar performance, indicating the robustness of MOBO-OSD with respect to n_{β} parameter.

Table 3: Number of required function evaluations to complete the first round of n_{β} NBI subproblems, including finding individual optima and solving n_{β} NBI subproblems. Gradient-based solver cost significantly more budget due to gradient computation via finite difference method. Generally, NBI depletes all 200 evaluation budget before finishing the first round of optimization.

	Individual Objectives	Subproblems (Gradient-free solver)	Subproblems (Gradient-based solver)
VLMOP2	139.20 ± 32.06	259.20 ± 32.06	8049.70 ± 1750.33
ZDT1-M2	24.00 ± 0.00	144.00 ± 0.00	720.20 ± 29.50
DTLZ2-M2	30.00 ± 9.30	150.00 ± 9.30	898.20 ± 22.52
DTLZ2-M3	36.60 ± 1.80	156.60 ± 1.80	1118.90 ± 213.97
DTLZ2-M4	54.00 ± 8.90	174.00 ± 8.90	2050.80 ± 1176.62
Speed Reducer	72.00 ± 25.04	232.00 ± 25.04	7680.70 ± 1023.34
Car Side Design	109.60 ± 10.15	269.60 ± 10.15	5141.30 ± 1105.41
Marine Design	139.30 ± 22.45	279.30 ± 22.45	7859.30 ± 1032.65
Water Planning	44.00 ± 0.00	124.00 ± 0.00	124.00 ± 0.00

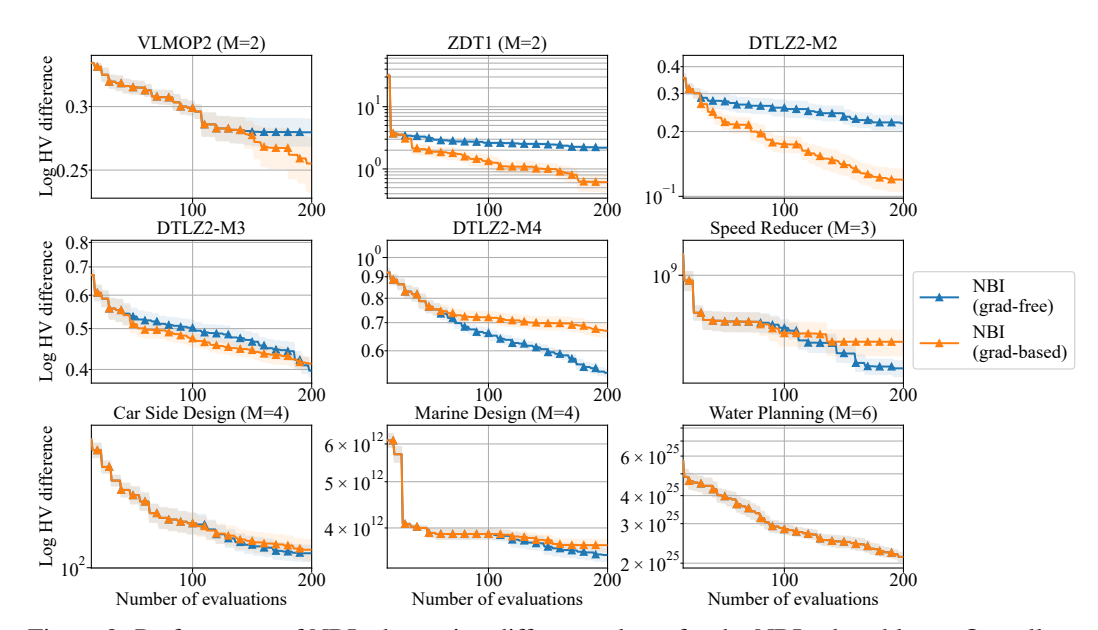


Figure 9: Performance of NBI when using different solvers for the NBI subproblems. Overall, no variant is consistently better than the other.

number of training samples, resulting in a computational complexity of $\mathcal{O}(N^3)$. The computational complexity for solving each MOBO-OSD subproblem is $\mathcal{O}(D^3+N^2n)$, which comprises of two dominated components: the SLSQP solver with cost of $\mathcal{O}(D^3)$, and the approximated cost of $\mathcal{O}(N^2n)$ associated with evaluating the mean vector, standard deviation vector, and their corresponding gradients. For the Pareto Front Estimation step, following Schulz et al. [46] and Konakovic Lukovic et al. [33], the computational cost is $\mathcal{O}(D^3+Nn)$. Finally, for the batch Hypervolume Improvement acquisition function, following Daulton et al. [13], the computational complexity is $\mathcal{O}(MK(2^b-1))$, where K is the number of disjoint partitions for box decompositions and b is the batch size.

Additionally, we provide the empirical runtime for the proposed method and all baselines in Tables 4, 5, 6 and 7 for batch size $b = \{1, 4, 8, 10\}$, respectively. Note that qEHVI is significantly more computationally (in terms of runtime and required memory) than other baselines and MOBO-OSD, especially when $b = \{8, 10\}$, hence can only have partial results on problems with $M \geq 4$ objectives. All NSGA-II runs cost less than 0.01s, so we exclude the method from the results. Moreover, symbol "-" indicates the method is not applicable for the corresponding baseline, according to the authors' implementation.

Table 4: Runtime comparison (seconds per iteration) for *batch size 1*. Overall, our proposed method, MOBO-OSD, have affordable time complexity. JES is significantly more computational expensive even in sequential setting. Symbol "-" indicates the method is not applicable for the corresponding benchmark problems.

	MOBO-OSD (Ours)	PDBO	qEHVI	JES	DGEMO	USeMO (EI)	qParEGO
VLMOP2	16.18	32.02	2.14	67.30	9.46	1.89	0.60
ZDT1-M2	7.50	22.47	1.89	40.67	11.84	2.28	0.50
DTLZ2-M2	8.34	23.74	2.95	46.99	8.74	1.91	0.50
DTLZ2-M3	11.72	15.38	10.32	53.69	10.63	2.75	0.68
DTLZ2-M4	19.85	14.66	55.27	126.97	-	3.75	0.88
Speed Reducer	17.18	13.38	6.91	115.07	16.31	2.67	0.71
Car Side Design	24.84	15.65	16.31	105.03	-	4.00	0.92
Marine Design	22.72	17.03	17.17	91.56	-	3.50	1.81
Water Planning	30.16	73.66	150.93	846.36	-	5.34	1.72

Table 5: Runtime comparison (seconds per iteration) for *batch size 4*. Overall, our proposed method, MOBO-OSD, have affordable time complexity. qEHVI is significantly more computational expensive with increasing batch size. Symbol "-" indicates the method is not applicable for the corresponding benchmark problems.

	MOBO-OSD (Ours)	PDBO	qEHVI	DGEMO	USeMO (EI)	qParEGO
VLMOP2	4.34	8.23	2.20	2.33	0.69	0.45
ZDT1-M2	2.31	5.86	1.63	2.81	0.65	0.39
DTLZ2-M2	2.51	7.23	2.60	2.13	0.53	0.39
DTLZ2-M3	3.80	4.95	8.82	2.86	0.78	0.52
DTLZ2-M4	10.58	4.45	31.73	-	1.14	0.65
Speed Reducer	4.65	3.84	14.06	3.96	0.72	0.53
Car Side Design	13.90	5.11	71.46	-	1.23	0.66
Marine Design	10.03	5.38	57.27	-	1.05	1.83
Water Planning	24.25	21.47	272.16	-	2.06	1.11

Table 6: Runtime comparison (seconds per iteration) for *batch size* 8. Overall, our proposed method, MOBO-OSD, have affordable time complexity. qEHVI is significantly more computational expensive with increasing batch size. Symbol "-" indicates the method is not applicable for the corresponding benchmark problems.

	MOBO-OSD (Ours)	PDBO	qEHVI	DGEMO	USeMO (EI)	qParEGO
VLMOP2	1.69	3.98	7.25	1.07	0.28	0.35
ZDT1-M2	1.11	3.05	4.47	1.35	0.42	0.34
DTLZ2-M2	1.14	3.56	10.00	1.03	0.33	0.34
DTLZ2-M3	1.71	2.22	100.07	1.43	0.55	0.46
DTLZ2-M4	2.42	2.33	449.26	-	0.66	0.56
Speed Reducer	2.42	2.36	66.35	2.16	0.36	0.46
Car Side Design	2.50	3.22	554.83	-	0.78	0.55
Marine Design	3.13	2.97	374.85	-	0.50	1.64
Water Planning	11.64	11.97	651.57	-	0.97	0.79

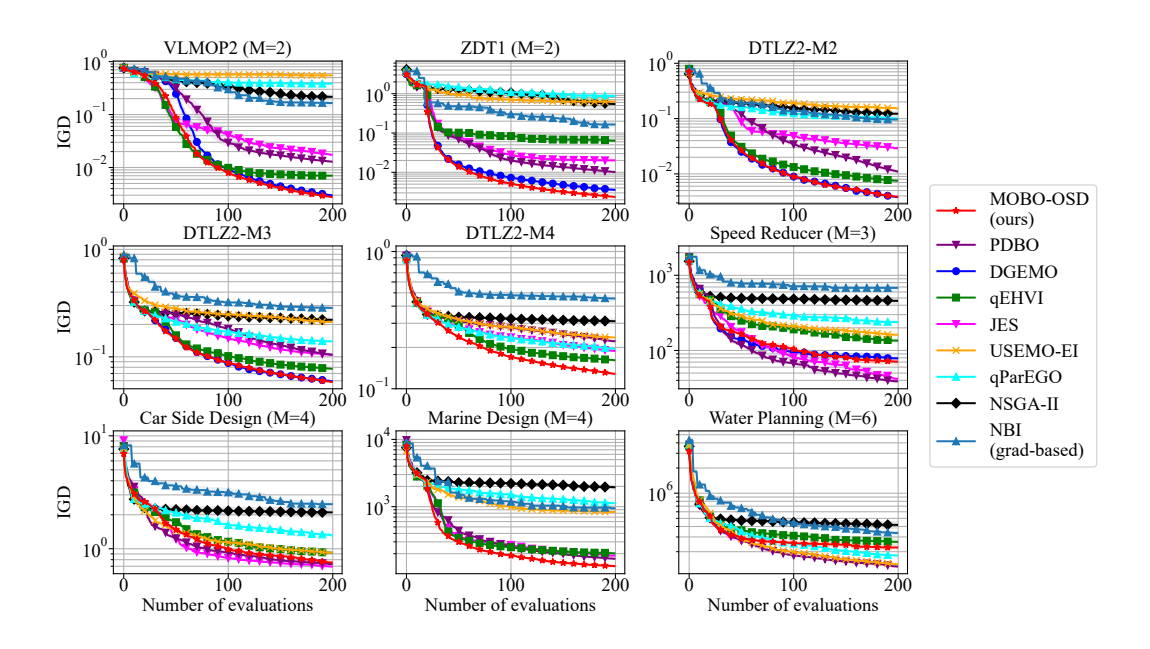


Figure 10: Comparison using *IGD indicator* of MOBO-OSD against the baselines on 5 synthetic and 4 real-world benchmark problems with batch size 1.

Table 7: Runtime comparison (seconds per iteration) for *batch size 10*. Overall, our proposed method, MOBO-OSD, have affordable time complexity. qEHVI is significantly more computational expensive with increasing batch size. Symbol "-" indicates the method is not applicable for the corresponding benchmark problems.

	MOBO-OSD (Ours)	PDBO	qEHVI	DGEMO	USeMO (EI)	qParEGO
VLMOP2	1.71	3.29	45.84	0.90	0.38	0.41
ZDT1-M2	1.13	2.57	18.72	1.11	0.67	0.41
DTLZ2-M2	1.15	2.92	57.72	0.82	0.45	0.40
DTLZ2-M3	1.78	1.89	229.09	1.25	0.46	0.55
DTLZ2-M4	2.73	2.07	446.87	-	1.00	0.70
Speed Reducer	2.49	1.89	158.63	1.67	0.42	0.54
Car Side Design	2.77	2.47	498.51	-	0.87	0.67
Marine Design	3.48	2.35	468.98	=	0.61	2.42
Water Planning	21.78	11.20	710.14	-	1.19	0.94

A.12 Other Comparison Metrics

We compare the performance of MOBO-OSD and the baselines using other comparison metrics, including IGD [10], IGD+ [25] and ε -indicator [60]. Figs 10, 11, 12 and 13 show the IGD metrics. Figs 14, 15, 16 and 17 show the IGD+ metrics. Figs 18, 19, 20 and 21 show the ε -indicator. Overall, MOBO-OSD shows competitive performance regardless of performance metrics.

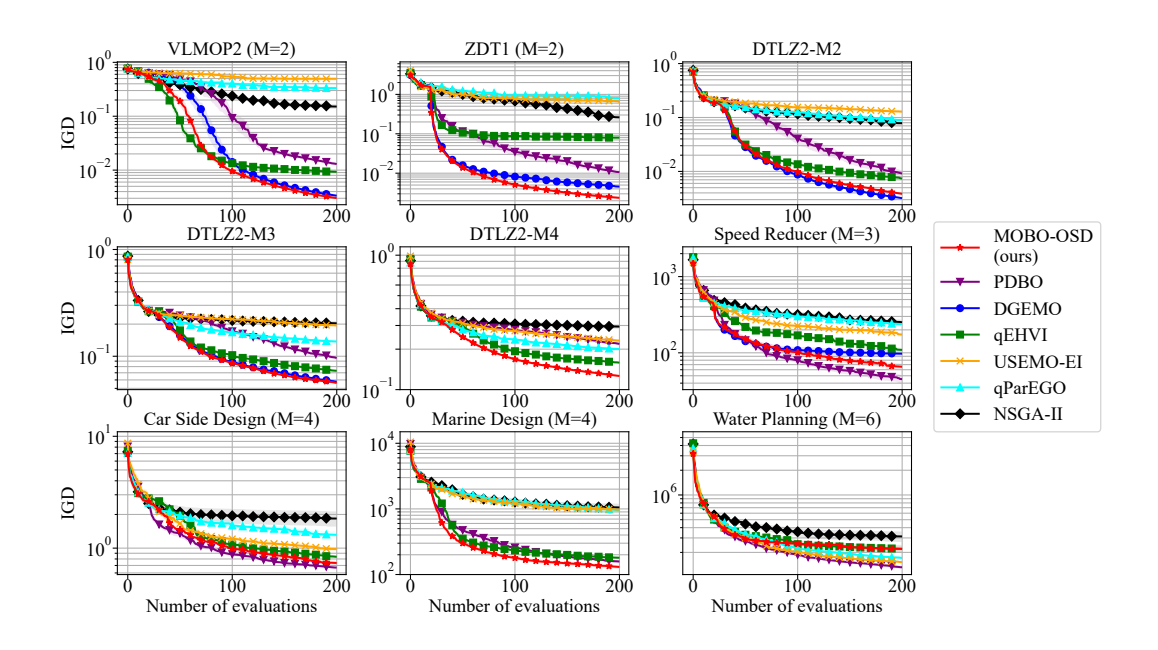


Figure 11: Comparison using *IGD indicator* of MOBO-OSD against the baselines on 5 synthetic and 4 real-world benchmark problems with batch size 4.

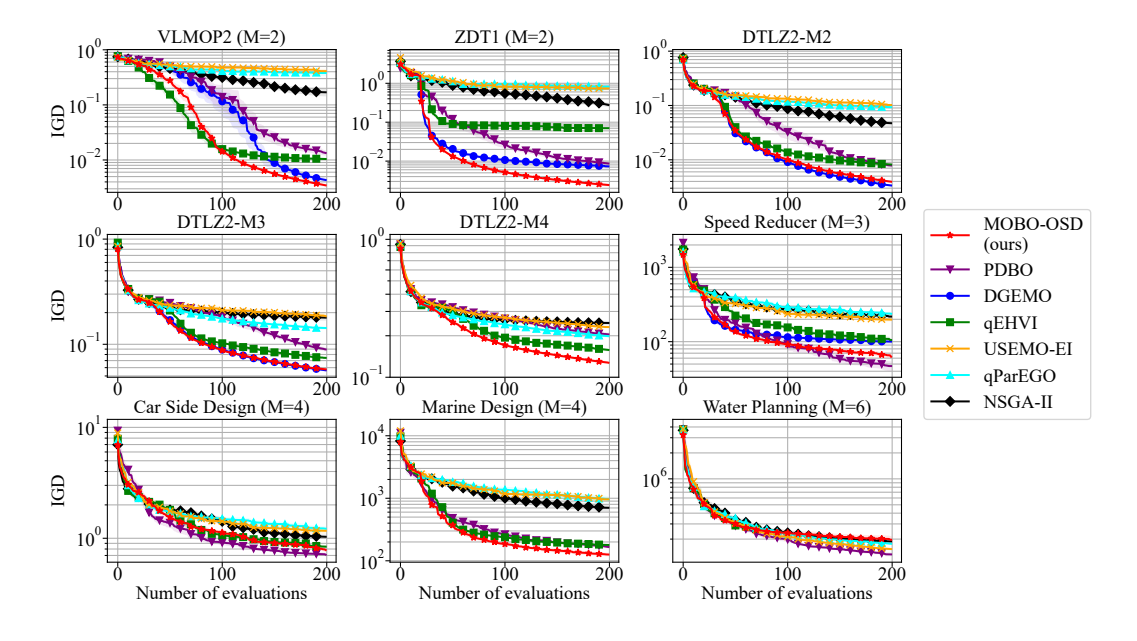


Figure 12: Comparison using *IGD indicator* of MOBO-OSD against the baselines on 5 synthetic and 4 real-world benchmark problems with batch size 8.

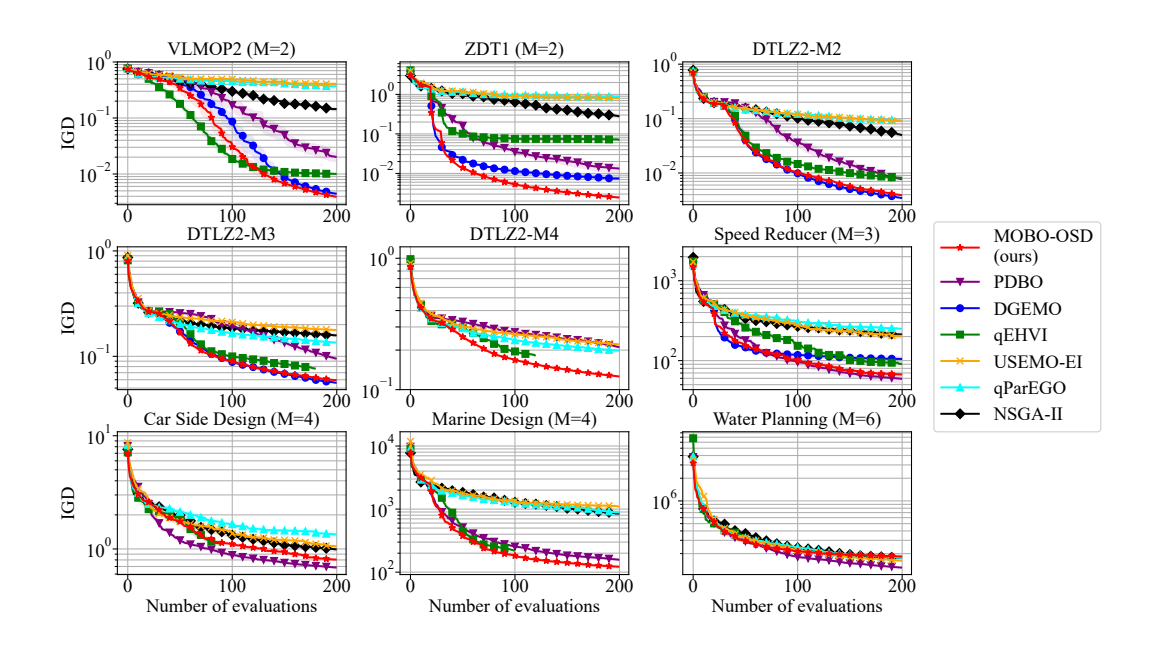


Figure 13: Comparison using *IGD indicator* of MOBO-OSD against the baselines on 5 synthetic and 4 real-world benchmark problems with batch size 10.

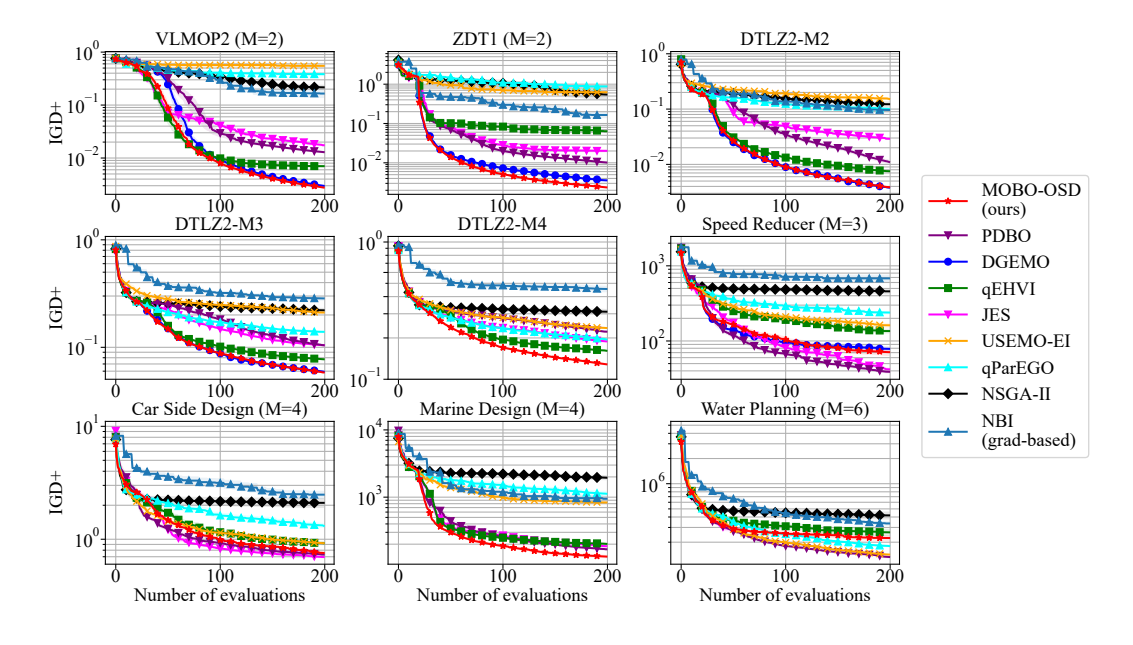


Figure 14: Comparison using *IGD+ indicator* of MOBO-OSD against the baselines on 5 synthetic and 4 real-world benchmark problems with batch size 1.

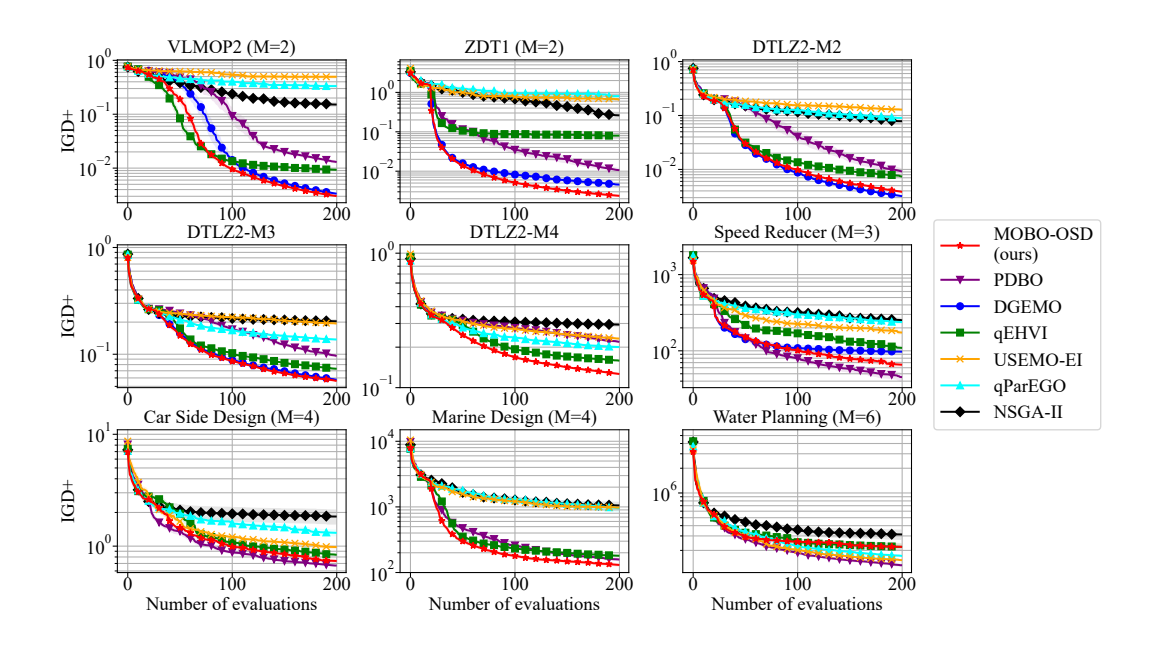


Figure 15: Comparison using *IGD+ indicator* of MOBO-OSD against the baselines on 5 synthetic and 4 real-world benchmark problems with batch size 4.

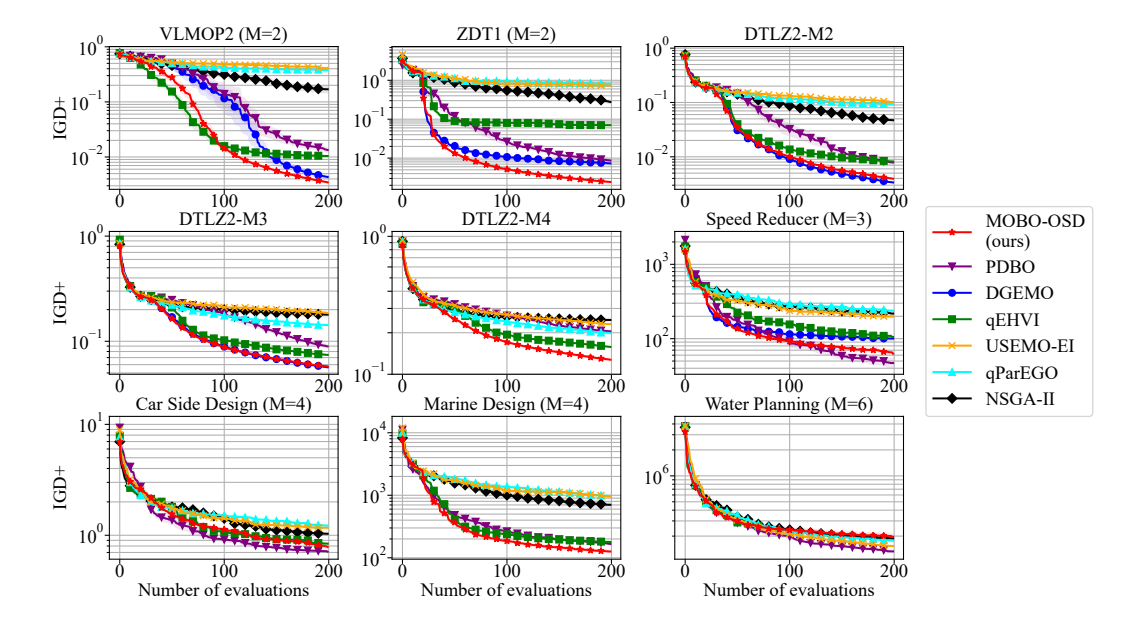


Figure 16: Comparison using *IGD+ indicator* of MOBO-OSD against the baselines on 5 synthetic and 4 real-world benchmark problems with batch size 8.

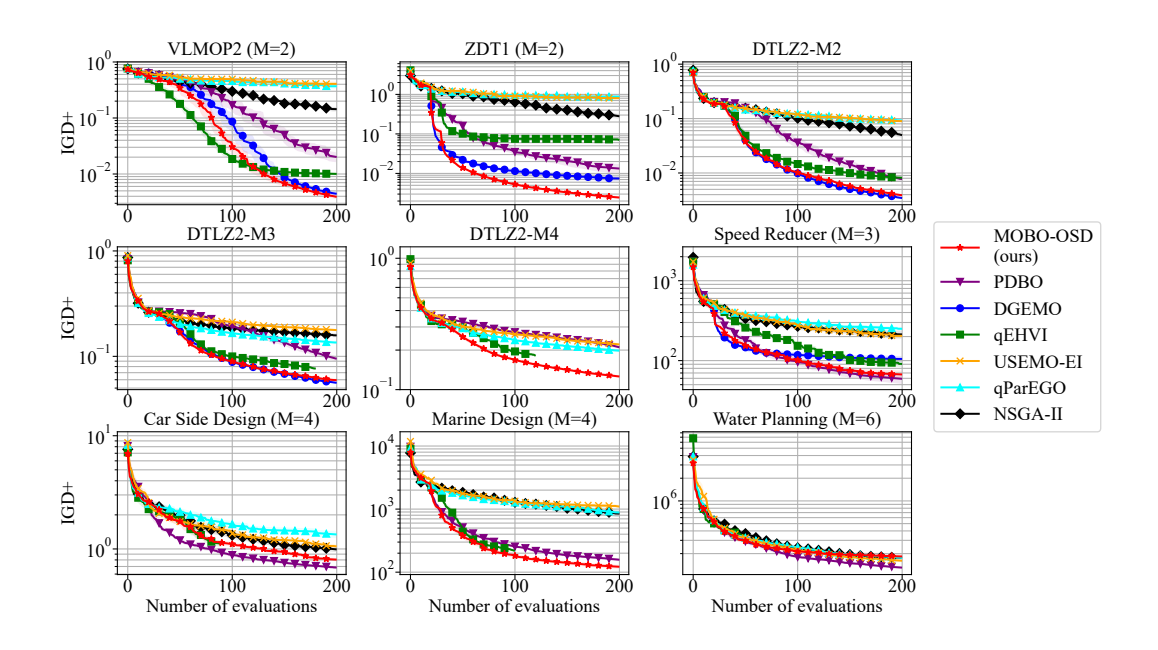


Figure 17: Comparison using *IGD+ indicator* of MOBO-OSD against the baselines on 5 synthetic and 4 real-world benchmark problems with batch size 10.

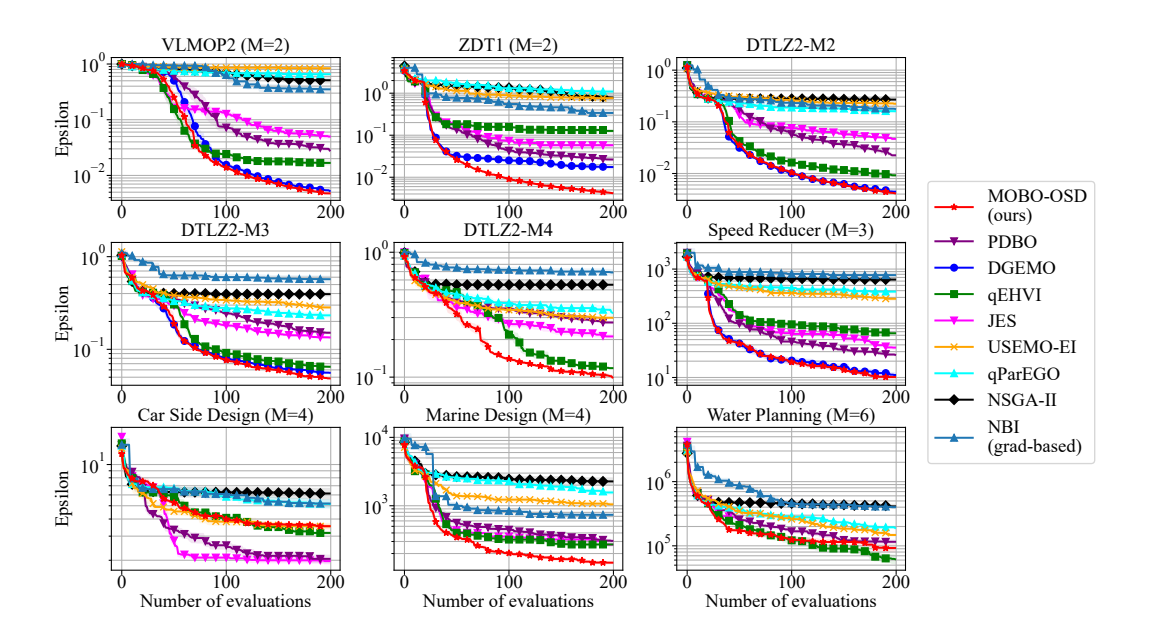


Figure 18: Comparison using ε -indicator of MOBO-OSD against the baselines on 5 synthetic and 4 real-world benchmark problems with batch size 1.

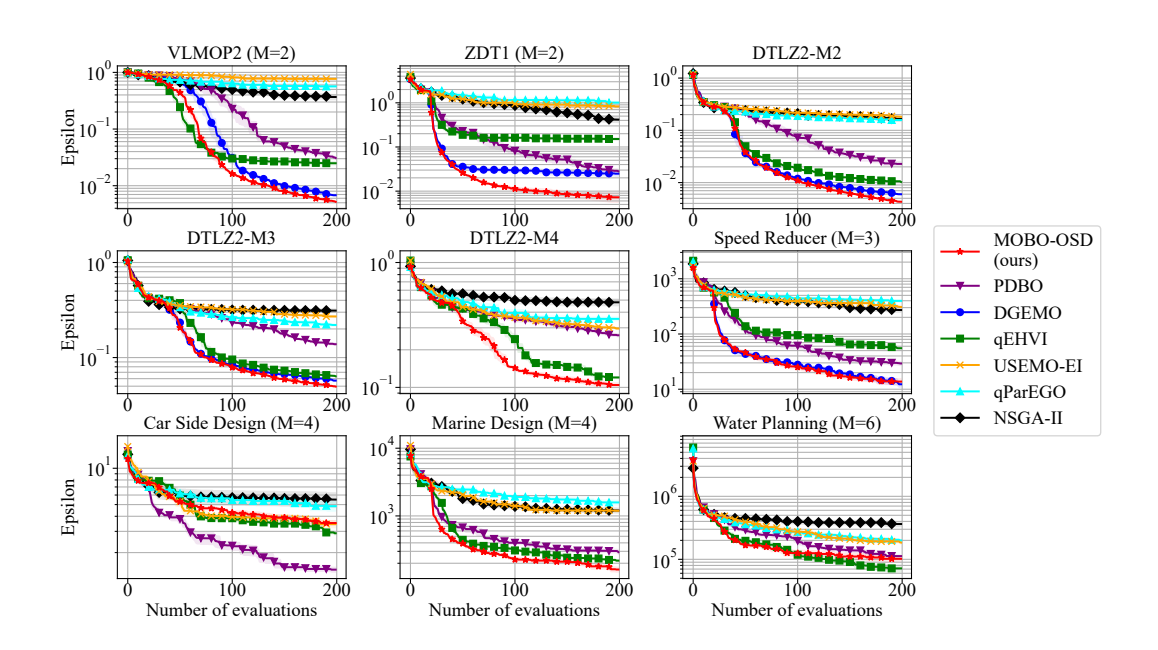


Figure 19: Comparison using ε -indicator of MOBO-OSD against the baselines on 5 synthetic and 4 real-world benchmark problems with batch size 4.

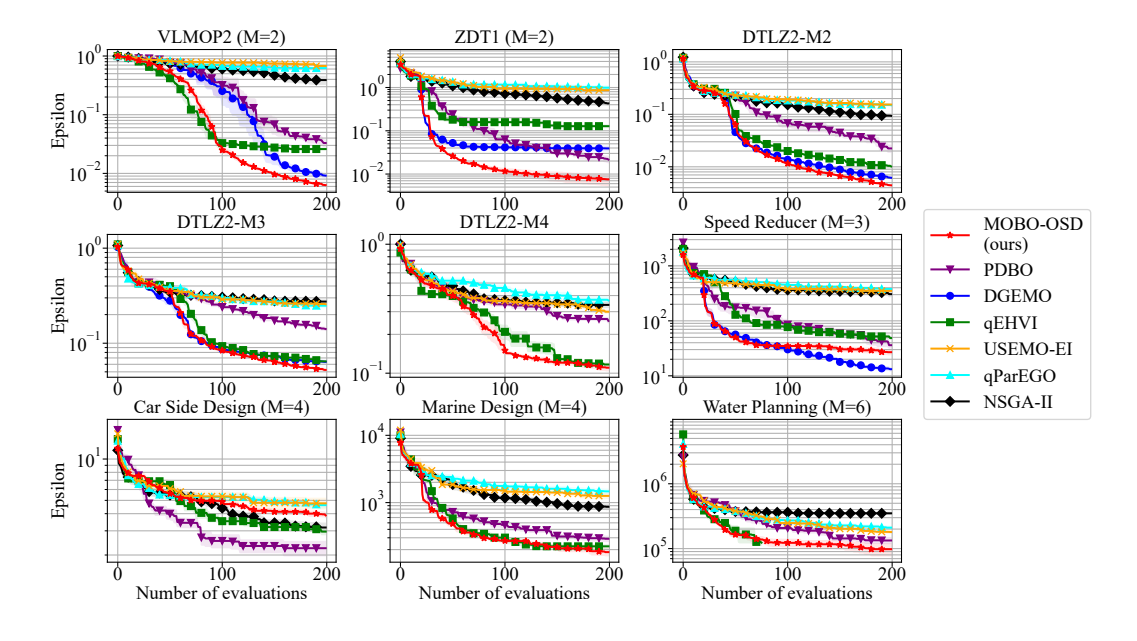


Figure 20: Comparison using ε -indicator of MOBO-OSD against the baselines on 5 synthetic and 4 real-world benchmark problems with batch size 8.

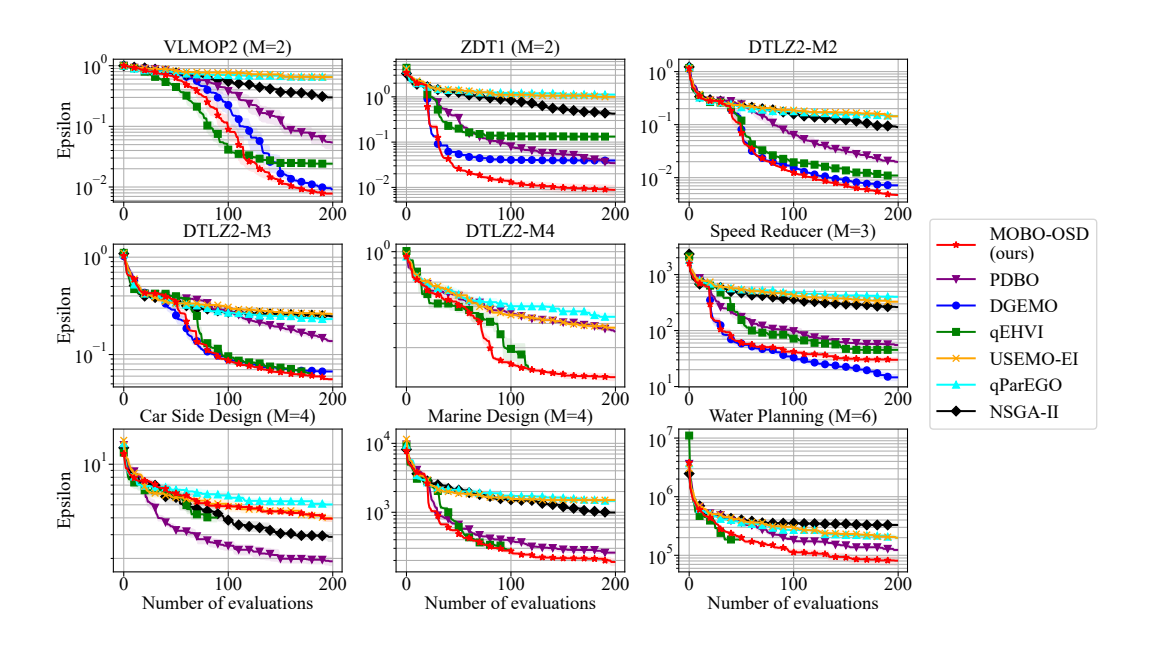


Figure 21: Comparison using ε -indicator of MOBO-OSD against the baselines on 5 synthetic and 4 real-world benchmark problems with batch size 10.